Supporting information

Polyoxoniobates as molecular building blocks in thin films

Mark A. Rambaran, András Gorzsás, Michael Holmboe and C. André Ohlin*

Department of Chemistry, Faculty of Science and Technology, Umeå University, 901 87 Sweden

*Corresponding author: andre.ohlin@umu.se

website: http://moleculargeo.chem.umu.se/ohlin

S1. Materials and method

Hydrous Nb_2O_5 was obtained as a gift from Prof. William H. Casey at UC Davis and used as is. Anhydrous niobium(V) oxide (99.99% trace metal basis, mixed polymorphs) was obtained from Sigma Aldrich. Titanium tetraisopropoxide (TTIP) 97%, H_2SO_4 97% and H_2O_2 30% were obtained from Sigma Aldrich. Tetramethylammonium hydroxide pentahydrate (TMAOH) 98% ($[N(CH_3)_4]OH{\cdot}5H_2O$) was obtained from Acros Organics. Silicon wafers (50.8 ±0.3 mm, 279 ±25 µm, p-doped, 10-20 Ω cm) were obtained from Siegert Wafer GmbH. All solutions/reactions used deionized water from the Elga Purelab Chorus water purification system (18.2 MΩ cm, 25 °C).

A Biotage Initiator$^+$ microwave synthesizer (400 W) was used for microwave irradiation synthesis. Similarly to the previous microwave synthesis of polyoxoniobates and –tantalates,[1] the general procedure for synthesis of decaniobate and hexaniobate followed: suspensions of $Nb_2O_5{\cdot}nH_2O$ in aqueous solutions of TMAOH being microwave irradiated at 180 °C in 10-20 mL sealed glass vials for 15 minutes, yielding autogenic pressures of 12-14 bars. After cooling the suspensions were filtered, the liquors kept and the products precipitated with isopropanol/acetonitrile or acetone. The synthesis of titanoniobates proceeded with microwave irradiation at 170-180 °C for 30 minutes, yielding similar autogenic pressures. After work-up and precipitation, the titanoniobates were extracted in methanol and the extract filtered through a 0.20 µm PTFE syringe filter to remove precipitated TiO_2.

S1.1 Polyoxometalate synthesis

S1.1.1 Microwave Irradiation Synthesis of Decaniobate $[N(CH_3)_4]_6[Nb_{10}O_{28}]{\cdot}2H_2O$

$Nb_2O_5{\cdot}nH_2O$ (4.00 g, 12.34 mmol; 82% w/w) was mixed with a solution of $[N(CH_3)_4]OH{\cdot}5H_2O$ (2.70 g, 14.9 mmol, 10 mL) and microwave irradiated at 180 °C for 15 minutes, resulting in a clear solution which was filtered through a 0.22 µm nitrocellulose filter to remove unreacted $Nb_2O_5{\cdot}nH_2O$. Acetone (20 mL) was added to precipitate the product and the supernatant was removed. This was repeated three times with 10 mL aliquots of acetone to precipitate a white powder which was filtered under suction, collected and oven-dried at 90 °C overnight under standard conditions to yield 3.25 g (71%) of $[N(CH_3)_4]_6[Nb_{10}O_{28}]{\cdot}2H_2O$. ^{17}O-NMR ($[Nb_{10}O_{28}]^{6-}$ H_2O, 25 °C): 306.6 ppm (μ_2-O; B), 465.3 ppm (μ_2-O; D), 471.5 ppm (μ_2-O; C), 552.9 ppm (μ_2-O; E), 703 ppm (η=O; G) and 720.9 ppm (η=O; F). Raman spectroscopy of the $[Nb_{10}O_{28}]^{6-}$ cluster in: (i) solution detected symmetric and asymmetric stretching of the terminal Nb=O at 930 cm^{-1} and 900 cm^{-1}, respectively; (ii) solid detected symmetric and asymmetric stretching of the terminal Nb=O at 919 cm^{-1} and 883 cm^{-1}, respectively.

S1.1.2 Microwave Irradiation Synthesis of Monotitanoniobate $[N(CH_3)_4]_7[TiNb_9O_{28}]{\cdot}3H_2O$

$Nb_2O_5{\cdot}nH_2O$ (3.00 g, 9.25 mmol; 82% w/w) and TTIP 97% (0.54 mL, 1.77 mmol) were mixed with a solution of $[N(CH_3)_4]OH{\cdot}5H_2O$ (2.5g, 13.8 mmol, 10 mL) and microwave irradiated at 180 °C for 30 minutes, resulting in a clear solution which was filtered through a 0.22 µm nitrocellulose filter to remove unreacted $Nb_2O_5{\cdot}nH_2O$ and TiO_2. Isopropanol (20 mL) was added to precipitate the product and the supernatant was removed. This was repeated five times with 10 mL aliquots of isopropanol to precipitate a white powder and acetonitrile (80 ml) was added to remove any

remaining water from the product. The acetonitrile was decanted and the product was extracted in methanol (10 mL).The synthesis was repeated three times and all the extracts were combined and filtered through a 0.20 µm PTFE syringe filter, prior to being dried in-*vacuo* to yield a white powder, 9.56 g (61%) of $[N(CH_3)_4]_7[TiNb_9O_{28}]\cdot 3H_2O$. ^{17}O-NMR ($[TiNb_9O_{28}]^{7-}$ H_2O, 25 °C): 299.8 ppm (μ_3-O; B_{Nb}), 340.2 ppm (μ_3-O; B_{Ti}), 452.5 ppm (μ_2-O; D), 458.3 ppm (μ_2-O; C_{Ti}), 462.2 ppm (μ_2-O; C_{Nb}), 545.9 ppm (μ_2-O; E_{Nb}), 592.6 ppm (μ_2-O; E_{Ti}), 670.2 ppm (η=O; G_{Ti}), 672.5 ppm (η=O; G_{Nb}) and 690.1 ppm (η=O; F). Raman spectroscopy of the $[TiNb_9O_{28}]^{7-}$ cluster in: (i) solution detected symmetric and asymmetric stretching of the terminal Nb=O at 917 cm^{-1} and 880 cm^{-1}, respectively; (ii) solid detected symmetric and asymmetric stretching of the terminal Nb=O at 904 cm^{-1} and 869 cm^{-1}, respectively.

S1.1.3 Microwave Irradiation Synthesis of Dititanoniobate $[N(CH_3)_4]_8[Ti_2Nb_8O_{28}]\cdot 6H_2O$

$Nb_2O_5\cdot nH_2O$ (3.00 g, 9.25 mmol; 82% w/w) and TTIP 97% (2.25 mL, 7.37 mmol) were mixed with a solution of $[N(CH_3)_4]OH\cdot 5H_2O$ (4.73g, 26.0 mmol, 10 mL) and microwave irradiated at 170 °C for 30 minutes, resulting in a clear solution which was filtered through a 0.22 µm nitrocellulose filter to remove unreacted $Nb_2O_5\cdot nH_2O$ and TiO_2. Isopropanol (20 mL) was added to precipitate the product and the supernatant was removed. This was repeated four times with 10 mL aliquots of isopropanol to precipitate a white powder and acetonitrile (80 ml) was added to remove any remaining water from the product. The acetonitrile was decanted and the product was extracted in methanol (30 mL).The synthesis was repeated five times and all the extracts were combined and filtered through a 0.20 µm PTFE syringe filter, prior to being dried in-*vacuo* to yield a white powder, 15.69 g (57%) of $[N(CH_3)_4]_8[Ti_2Nb_8O_{28}]\cdot 6H_2O$. ^{17}O-NMR ($[Ti_2Nb_8O_{28}]^{8-}$ H_2O, 25 °C): 433.3 ppm (μ_2-O; D), 449.8 ppm (μ_2-O; C), 579.9 ppm (μ_2-O; E), 644.1 ppm (η=O; G) and 662.8 ppm (η=O; F). Raman spectroscopy of the $[Ti_2Nb_8O_{28}]^{8-}$ cluster in: (i) solution detected symmetric and asymmetric stretching of the terminal Nb=O at 905 cm^{-1} and 868 cm^{-1}, respectively; (ii) solid detected symmetric and asymmetric stretching of the terminal Nb=O at 888 cm^{-1} and 853 cm^{-1}, respectively.

S1.2 Substrate preparation

Silicon wafers were cleaved into ca. 2.5 cm circular quadrants and soaked in H_2SO_4 (97%) and H_2O_2 (30%) mixed in a 3:1 ratio – henceforth referred to as piranha solution – with stirring overnight, followed by liberal washing with water, then dried on a hotplate at 200 °C for ca. 15 minutes. Thereafter the substrates were treated with air plasma for 15 minutes inside a Diener Zepto-W6 plasma cleaner (85% power and pressure of 0.6 mbar). Prior to spin coating, clear cellophane tape (2.5 cm x 0.4 cm) was placed along one side of the circular quadrant to preserve an uncoated region of the substrate during spin coating. For depositing successive layers, the coated substrate was treated with air plasma similarly for 30 minutes and clear cellophane tape was added to preserve an uncoated region of the substrate, prior to the spin coating process.

S1.3 Thin film formation

A SPS spin coater (SPS Europe) was used for spin coating. Pre-treated substrates were mounted and held under vacuum onto the spin coater substrate holder, followed by addition of the POM solution (100 µL) to the center of the substrate. The substrate was then rotated at 2000 rpm for 4

minutes. The tape was subsequently removed from the coated substrate, which was then annealed under standard atmospheric conditions at selected temperatures: 200 °C, 400 °C, 800 °C and 1000 °C using a Nabertherm LT 15/11 furnace (Nabertherm GmbH). The ramp rate was 5.0 °C min^{-1} for temperatures <1000 °C and 1.8 °C min^{-1} at 1000 °C and the final temperature was maintained for one hour prior to annealing. The solid POMs were annealed under the same conditions.

S1.4 Raman spectroscopy

For solid Raman spectroscopy of the synthesised and annealed POMs (ca. 0.4 g), Raman spectra (6 scans, co-added for good signal-to-noise ratios) were collected at 50 mW with the 532 nm laser and automatically background corrected with the Anton-Paar software (Cora 500 V2.0.4.5). Solution Raman spectroscopy used the same procedure but with 0.5 mL of the POM solution.

Raman microspectroscopy (mapping) was performed on a Renishaw Qontor Raman spectrometer 405 nm laser at 100% power and 0.2 s irradiation time set in the software (WIRE, v.5.3; Renishaw), in static mode, centered at 520 cm^{-1}. For mapping, a 100x non-immersive lens was used with 1 µm step sizes (in both X and Y directions), in high confocal modes recording images with a minimum of 2500 spectra. Raman shifts were calibrated using the built-in Si standard of the instrument. Cosmic rays were removed and data noise filtered using the chemometrics package of WIRE. Spectra were exported as .txt files and pre-processed using the open-source MCR-ALS script (run in MATLAB v.21b, MathWorks, CA, USA), as provided by the Vibrational Spectroscopy Core Facility (https://www.umu.se/en/research/infrastructure/visp/downloads/). Spectra were cut to the 100 – 1100 cm^{-1} region to remove noise filtering artefacts, and thereafter baseline corrected, smoothed and point max normalised (520 cm^{-1}).

S1.5 PXRD measurements

The powders and annealed films of the POMs were identified by randomly-oriented powder X-ray diffraction (XRD) measurements using PANalytical X'pert3 diffractometer (CuK-α radiation 1.54187 Å). The powdered samples were loaded onto a 1.5 cm circular cavity holder and run using a flat stage with the following parameters: 10-60º 2θ, 0.039º step size, 1 s collecting time, 45 kV, 40 mA, 0.04 rad Soller slits, 1/16º incident divergence slit, 5 mm anti-scattering receiving slit, and 10 mm mask. The divergence slit and mask were chosen so that the sample occupied the whole X-ray irradiated area. Diffractograms were baseline corrected using X'pert highscore and Rietveld refinement was done with Profex 4.2.[2]

S1.6 AFM imaging

AFM imaging was performed by using a BioScope Catalyst AFM (Bruker), operating in a peak force mode in air. The scan rate was 0.1 Hz and resolution was 512 x 512 pixels over a 10 µm x 10 µm scan area. A Bruker SLN cantilever was used in all measurements. Roughness was calculated over a 5 µm x 5 µm scan area using the Bruker Nansoscope analysis v.1.9 software.

S1.7 Ellipsometry measurements

Spectroscopic ellipsometry measurements were done using an Alpha-SE Ellipsometer (J.A. Woollam Co. Inc.) with single scans at 70.078° in long acquisition mode. The ellipsometric data was acquired and modelled with the CompleteEase v.5.23 software. Film thickness was calculated

using a B-spline curve derived from the "Global Fit" function associated with the *"Si with Absorbing Film.mod"* model used to fit the ellipsometric data.

S1.8 SEM measurements

The powdered and thin-film samples were attached onto carbon tape-mounted on aluminium stub. The surface morphology was examined by field-emission scanning electron microscopy (FESEM; Carl Zeiss Merlin) using in-lens secondary electron detector at accelerating voltage of 5 kV and probe current of 120 pA. The elemental composition analysis was performed using an energy dispersive X-ray spectrometer (EDS; Oxford Instruments X-Max 80 mm2) at accelerating voltage of 10 kV, probe current of 300 pA and acquisition time of 150 us (map analysis) and 30 s (area analysis). A dual-beam focused ion beam-scanning electron microscopy (FIB-SEM; Thermo Fisher Scientific Scios) is employed to expose the cross-section of the thin-film samples using gallium ion voltage of 30 kV and current in the range of 30-300 pA.

S1.9 UV-Vis measurements

UV-Visible spectroscopy was done using the PerkinElmer Lambda 750 UV/Vis/NIR Spectrometer (PerkinElmer, Inc., USA) equipped with a Deuterium and Tungsten halogen light source in Diffuse reflectance mode. Thin-film samples are mounted within the sample chamber and measurements were made from 700 to 250 nm under standard atmospheric conditions.

S2. Raman spectroscopy

S2.1 Raman spectra of Polyoxometalates

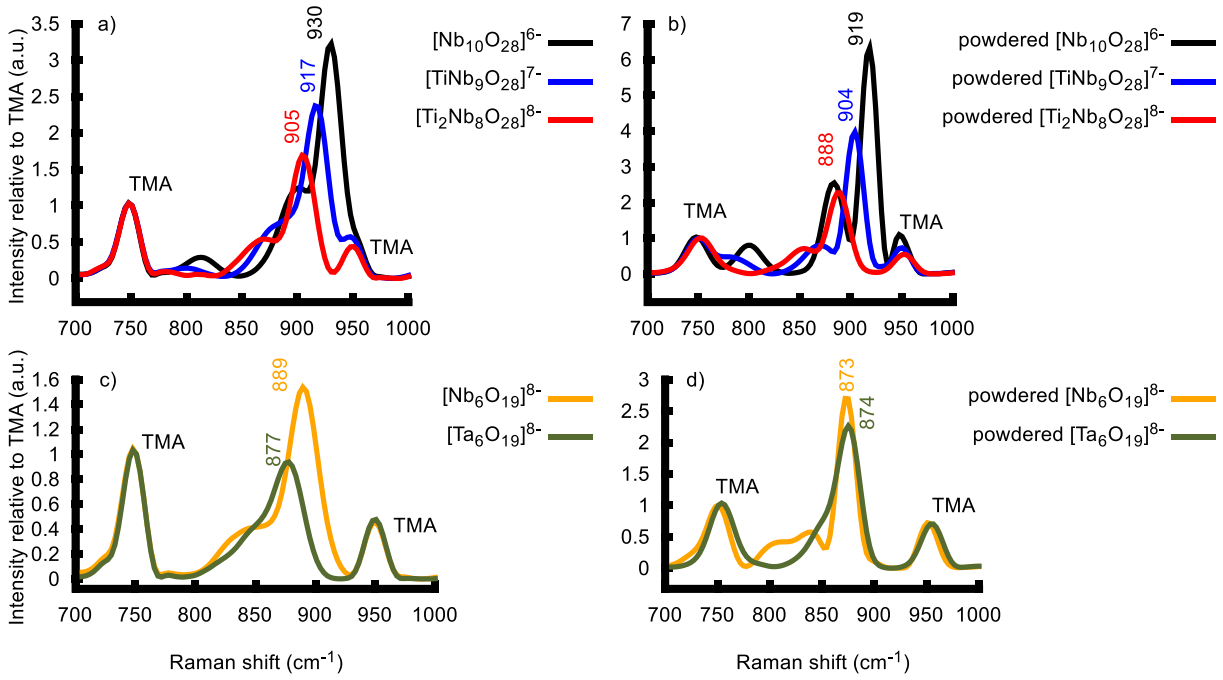

Figure S2-1. Raman spectra of $[Nb_{10}O_{28}]^{6-}$, $[TiNb_9O_{28}]^{7-}$ and $[Ti_2Nb_8O_{28}]^{8-}$ in solution (a) and solid (b) phase; $[Nb_6O_{19}]^{8-}$ and $[Ta_6O_{19}]^{8-}$ in solution (c) and solid (d) phase. Spectra are normalized against the TMA signal at 750 cm^{-1}.

S2.2 Raman spectra of annealed polyoxometalates

Table S2-1. Raman shifts of niobium pentoxide polymorphs, titanium-niobium oxides and tantalum pentoxide.

Compound/ POM	Annealing temperature (°C)	Bond type and Raman shifts (cm^{-1})				Crystal system	Structure form
		M=O	MO_6	μ_2-O[b],	μ_3-O[c]		
Hydrous Nb_2O_5	-	-	655	227, 245 395, 445 495	-	amorphous	-
Hydrous Ta_2O_5	-	-	653	346, 420 492	-	amorphous	-
Anhydrous Nb_2O_5	-	990, 900	719, 672, 620	834, 245	455	M[d], O[e]	$Nb_{12}O_{29}$, $Nb_{16.8}O_{42}$
$[Nb_{10}O_{28}]^{6-}$	800	-	682	300, 230	-	O[e]	$Nb_{16.8}O_{42}$
$[TiNb_9O_{28}]^{7-}$	800	996, 890	655	818, 533 255	455	M[d], O[e]	$Ti_2Nb_{10}O_{29}$
$[Ti_2Nb_8O_{28}]^{8-}$	800	998, 885	638	830, 527 243	446	M[d]	$TiNb_2O_7$
$[Nb_6O_{19}]^{8-}$	800	-	683	300, 230	-	O[e]	$Nb_{16.8}O_{42}$
$[Ta_6O_{19}]^{8-}$	800	-	700, 620	895, 845 476, 395 345, 246	-	O[e]	Ta_2O_5
$[Nb_{10}O_{28}]^{6-}$	1000	991, 896	660, 620	836, 540 246	456	M[d]	$Nb_{12}O_{29}$
$[TiNb_9O_{28}]^{7-}$	1000	996, 890	637	818, 533 255	455	M[d], O[e]	$Ti_2Nb_{10}O_{29}$
$[Ti_2Nb_8O_{28}]^{8-}$	1000	998, 885	638	830, 527 255	446	M[d]	$TiNb_2O_7$
$[Nb_6O_{19}]^{8-}$	1000	992, 895	660, 620	835, 544 256	460	M[d]	$Nb_{12}O_{29}$
$[Ta_6O_{19}]^{8-}$	1000	-	700, 620	895, 845 476, 395 345, 246	-	O[e]	Ta_2O_5

[a] M = Nb or Ta, [b] M-O-M bond, [c] O-M_3 bond, [d] Monoclinic, [e] Orthorhombic

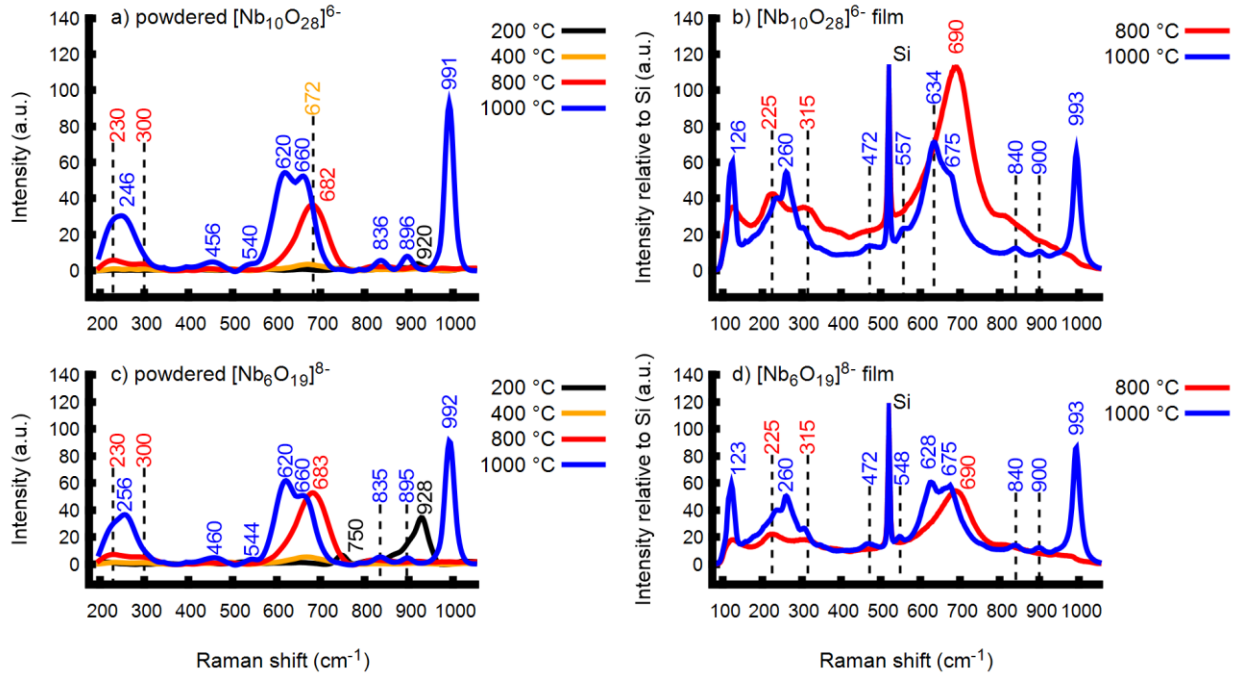

Figure S2-2. Raman spectra of powdered $[Nb_{10}O_{28}]^{6-}$ annealed at 200 – 1000 °C (a), $[Nb_{10}O_{28}]^{6-}$ film annealed at 800 °C and 1000 °C (b), Raman spectra of powdered $[Nb_6O_{19}]^{8-}$ annealed at 200 – 1000 °C (c) and $[Nb_6O_{19}]^{8-}$ film annealed at 800 °C and 1000 °C (d).

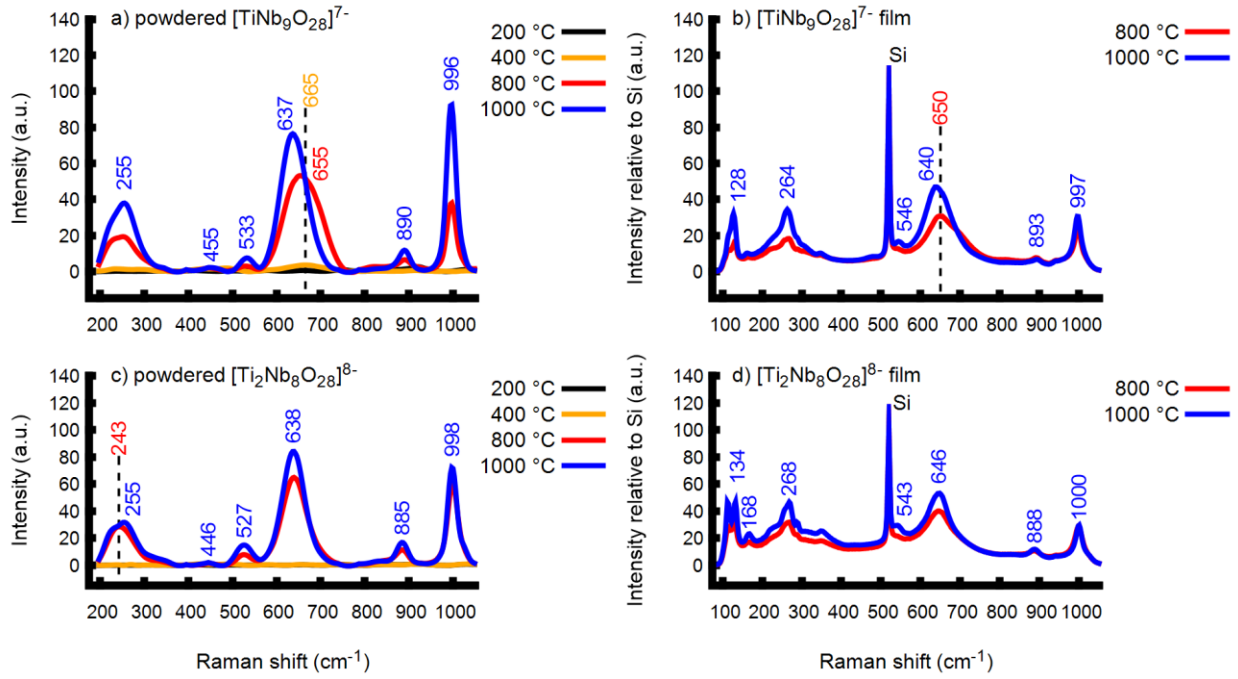

Figure S2-3. Raman spectra of powdered $[TiNb_9O_{28}]^{7-}$ annealed at 200 – 1000 °C (a), $[TiNb_9O_{28}]^{7-}$ film annealed at 800 °C and 1000 °C (b), Raman spectra of powdered $[Ti_2Nb_8O_{28}]^{8-}$ annealed at 200 – 1000 °C (c) and $[Ti_2Nb_8O_{28}]^{8-}$ film annealed at 800 °C and 1000 °C (d).

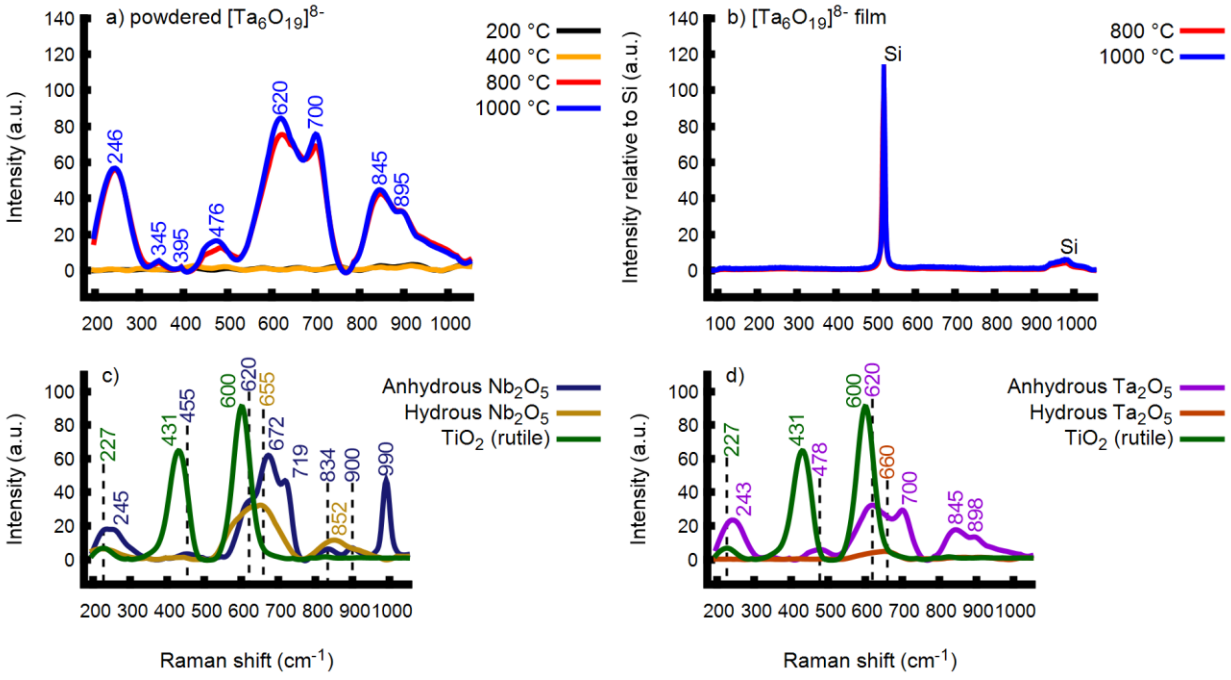

Figure S2- 4. Raman spectra of powdered $[Ta_6O_{19}]^{8-}$ annealed at 200 – 1000 °C (a) and $[Ta_6O_{19}]^{8-}$ film annealed at 800 °C and 1000 °C (c), Raman spectra of anhydrous Nb_2O_5, hydrous Nb_2O_5 and TiO_2 (c) and Raman spectra of anhydrous Ta_2O_5, hydrous Ta_2O_5 and TiO_2 (d).

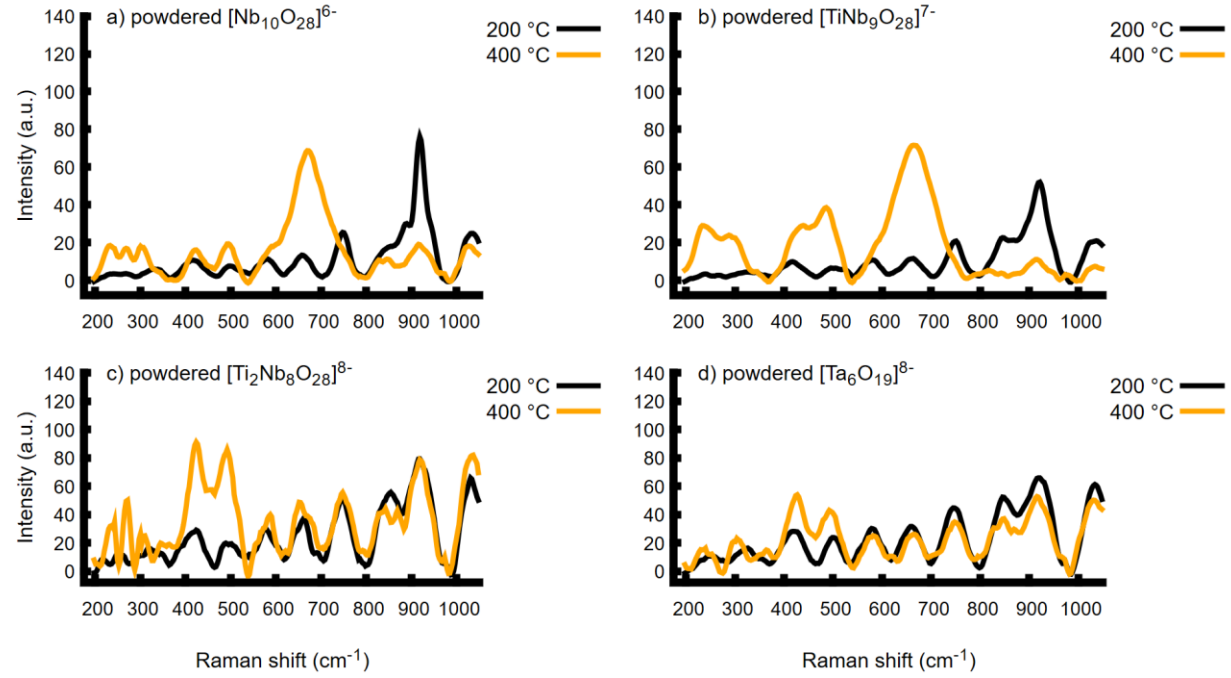

Figure S2- 5. Raman spectra of powdered (a) $[Nb_{10}O_{28}]^{6-}$, (b) $[TiNb_9O_{28}]^{7-}$, (c) $[Ti_2Nb_8O_{28}]^{8-}$ and (d) $[Ta_6O_{19}]^{8-}$ annealed at 200 – 400 °C.

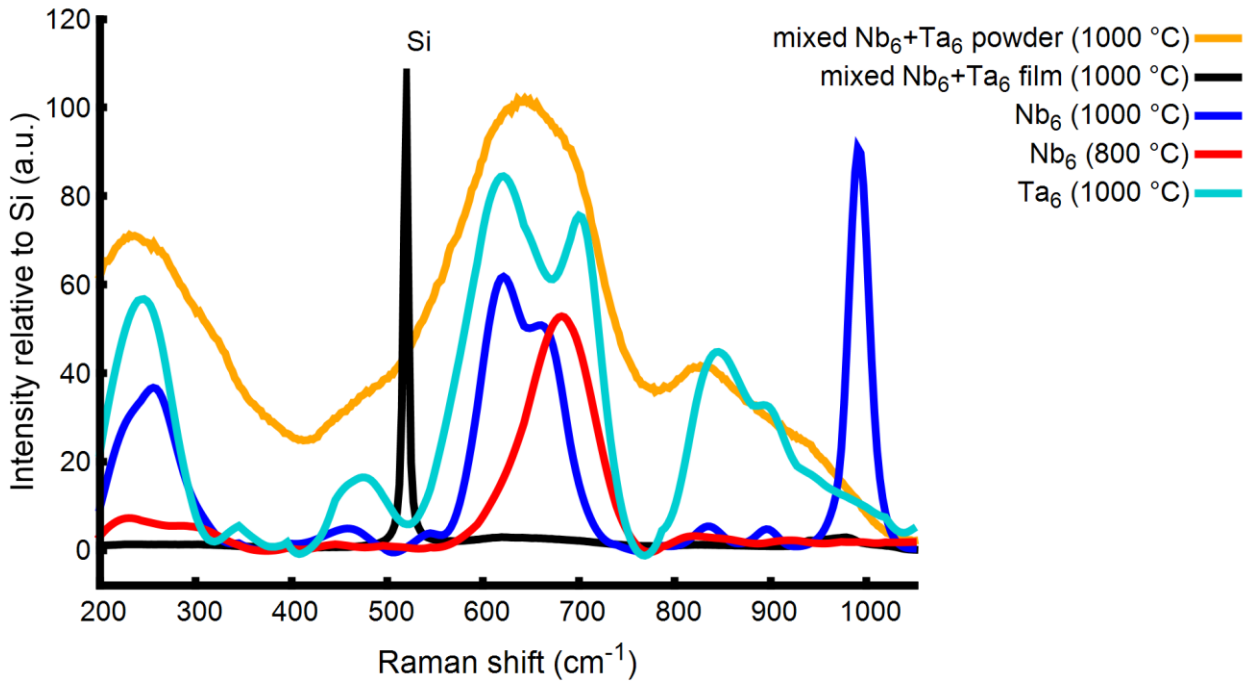

Figure S2- 6. Raman spectra of the film and powder obtained from a mixed-equimolar solution (0.2 M) of Nb_6 and Ta_6 annealed at 1,000 °C.

S3. Powder XRD

S3.1 Polyoxometalates

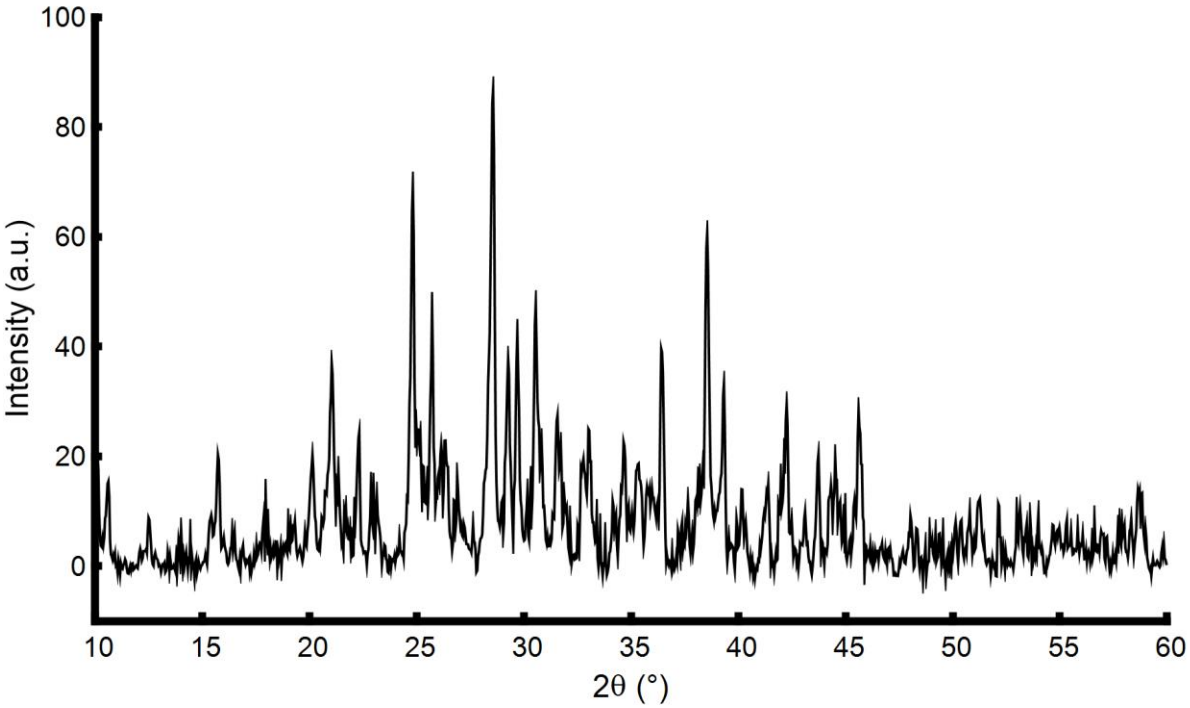

Figure S3-1. PXRD pattern of powdered $[Nb_{10}O_{28}]^{6-}$.

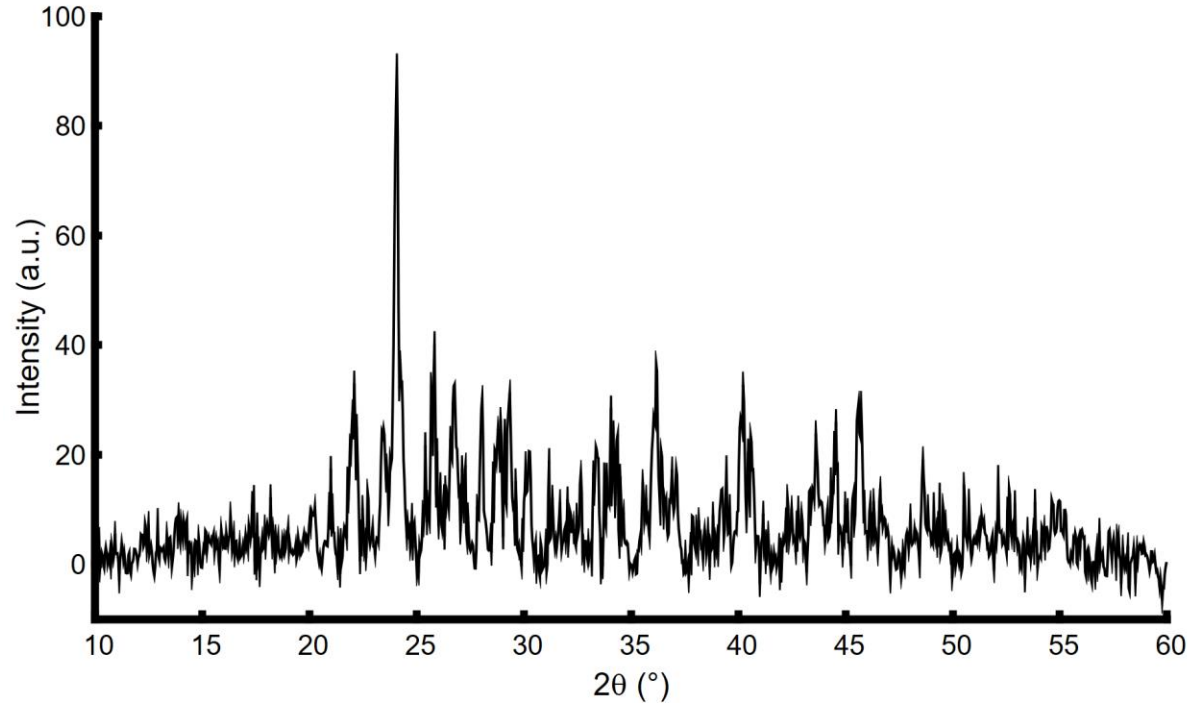

Figure S3-2. PXRD pattern of powdered $[Nb_6O_{19}]^{8-}$.

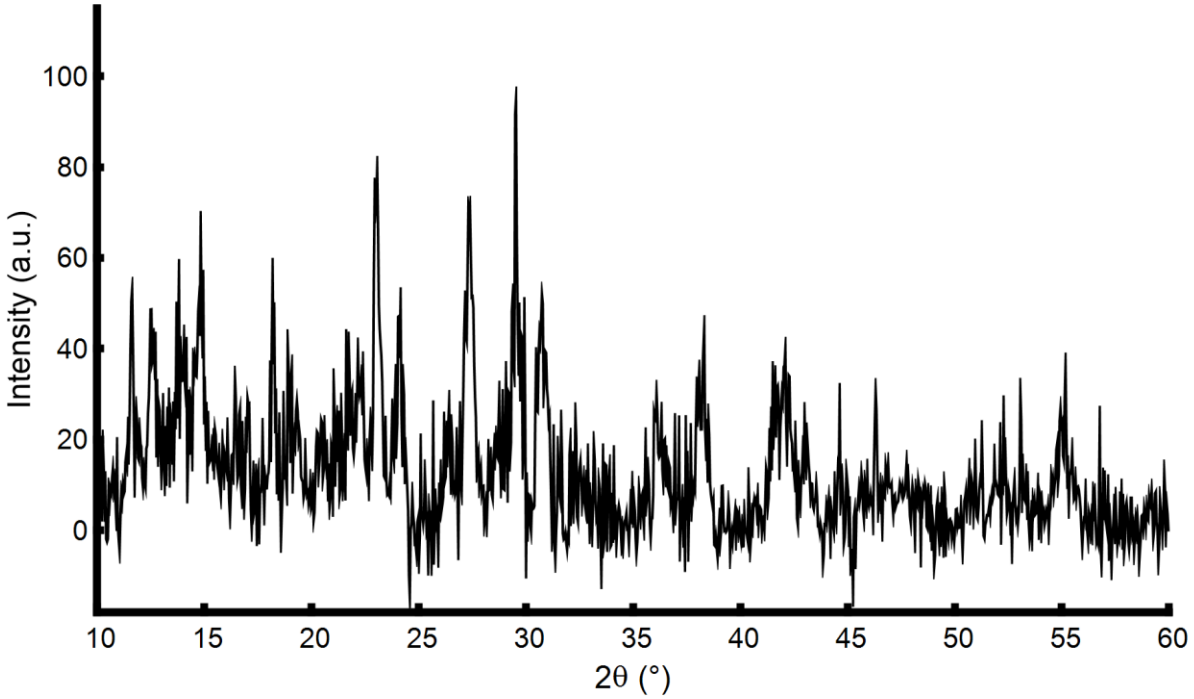

Figure S3-3. PXRD pattern of powdered $[TiNb_9O_{28}]^{7-}$.

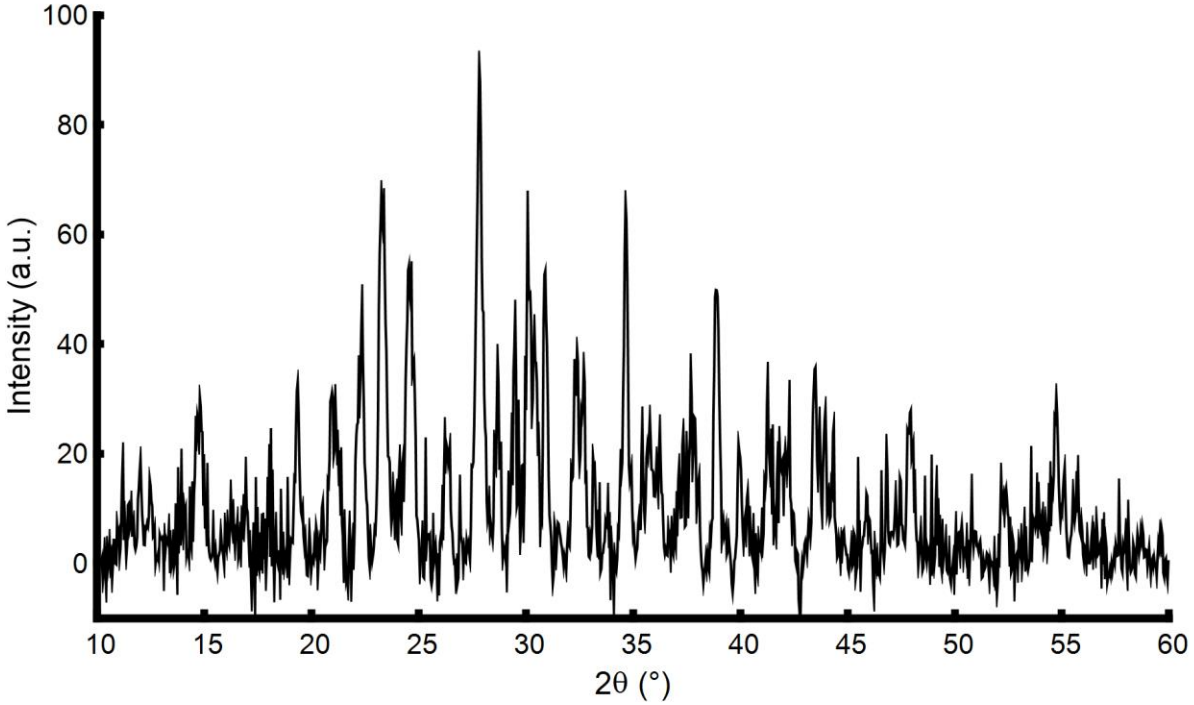

Figure S3-4. PXRD pattern of powdered $[Ti_2Nb_8O_{28}]^{8-}$.

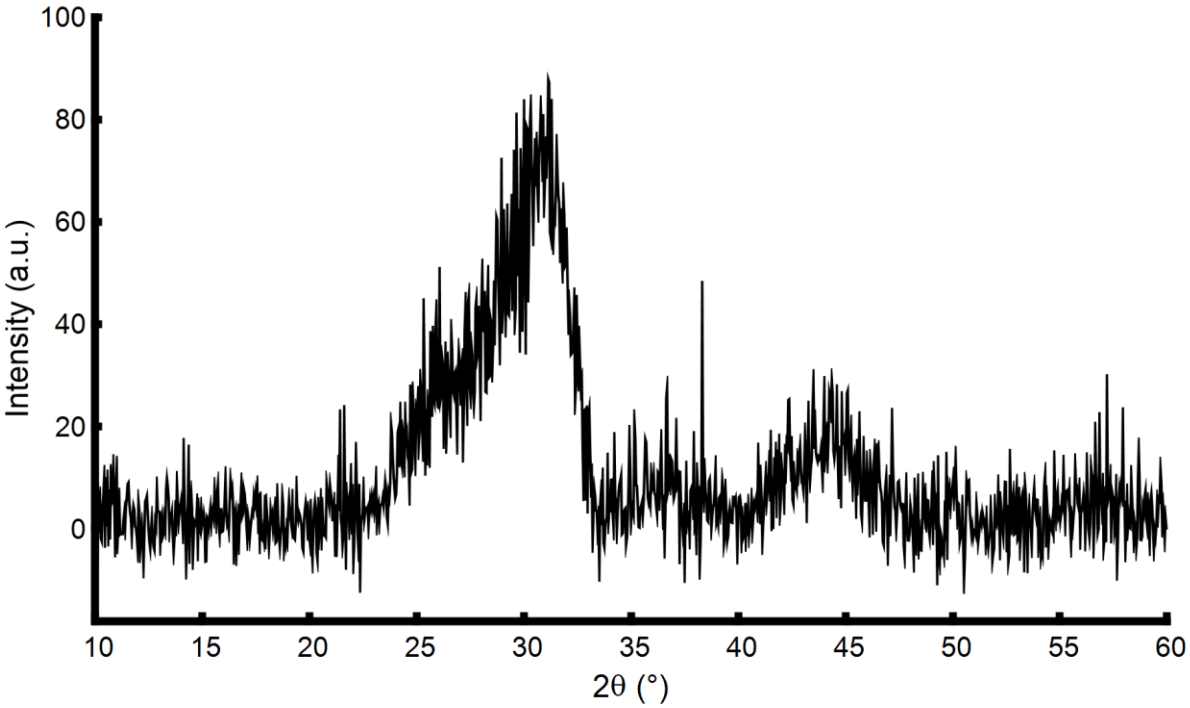

Figure S3-5. PXRD pattern of powdered $[Ta_6O_{19}]^{8-}$.

S3.2 Niobium and tantalum pentoxides

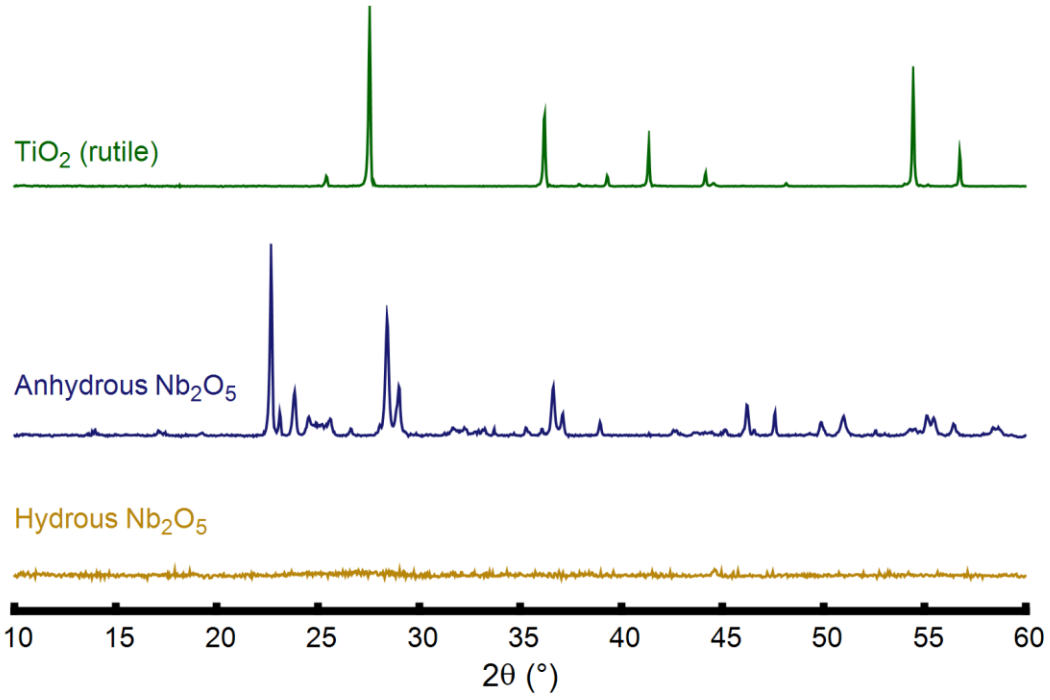

Figure S3-6. PXRD patterns of anhydrous Nb_2O_5, hydrous Nb_2O_5 and TiO_2 (rutile).

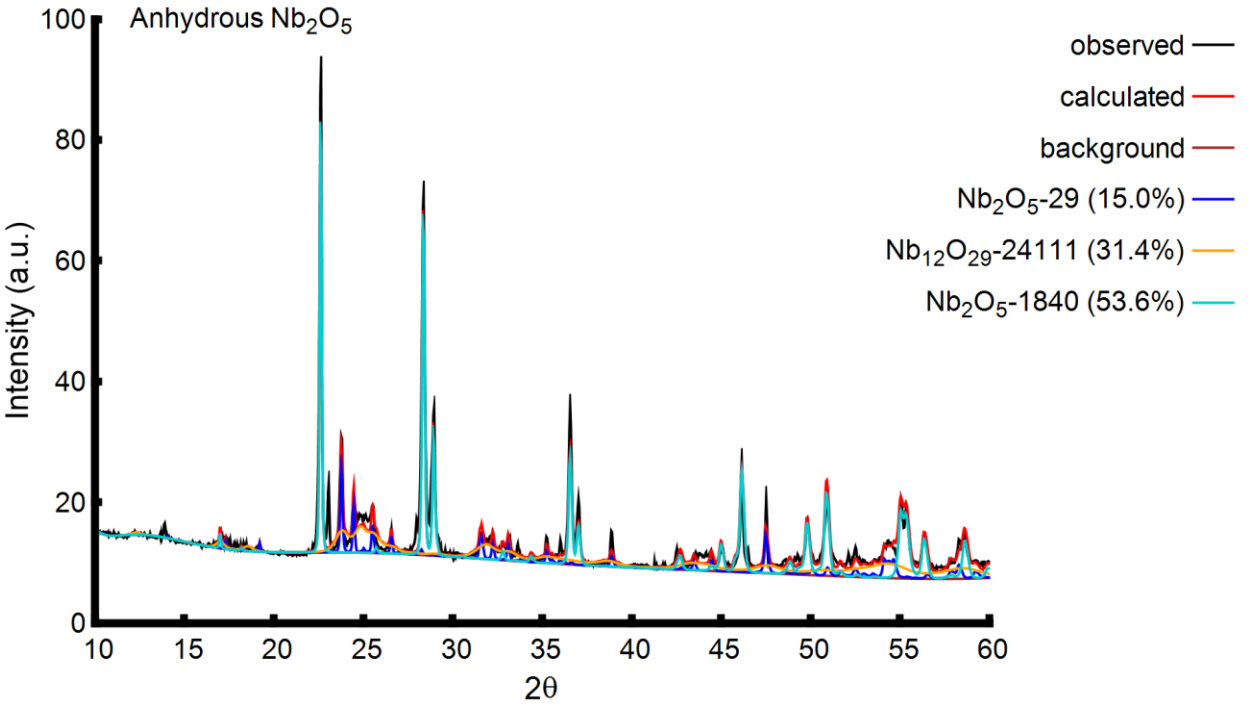

Figure S3-7. Rietveld refinement of the PXRD pattern of anhydrous Nb_2O_5. Nb_2O_5-29 and $Nb_{12}O_{29}$-24111 are monoclinic phases of Nb_2O_5; Nb_2O_5-1840 is the orthorhombic phase of Nb_2O_5.

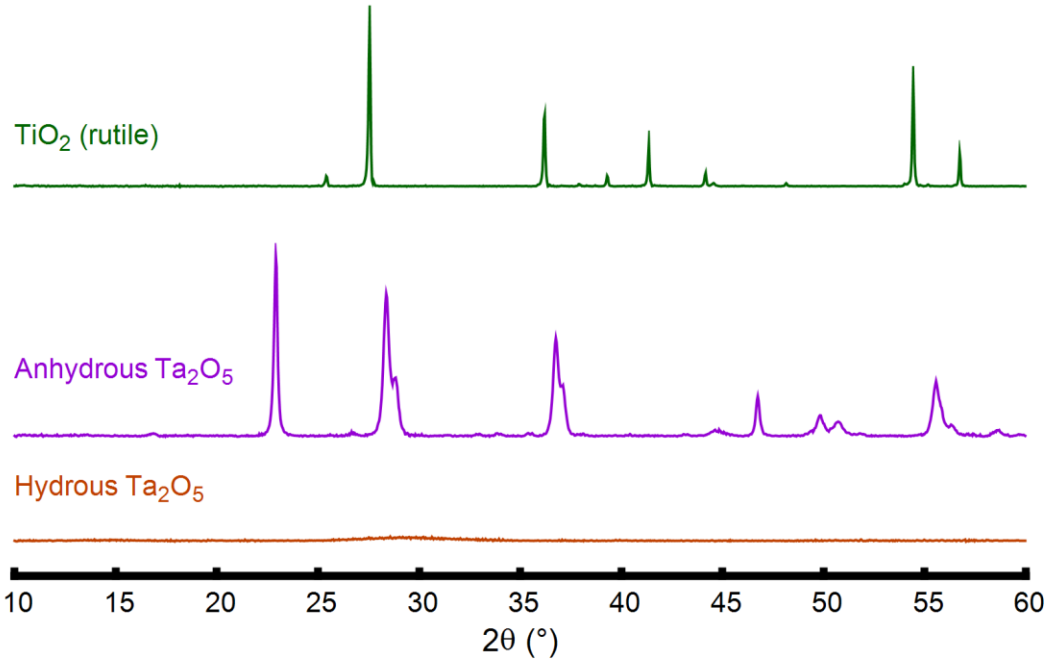

Figure S3-8. PXRD patterns of anhydrous Ta_2O_5, hydrous Ta_2O_5 and TiO_2 (rutile).

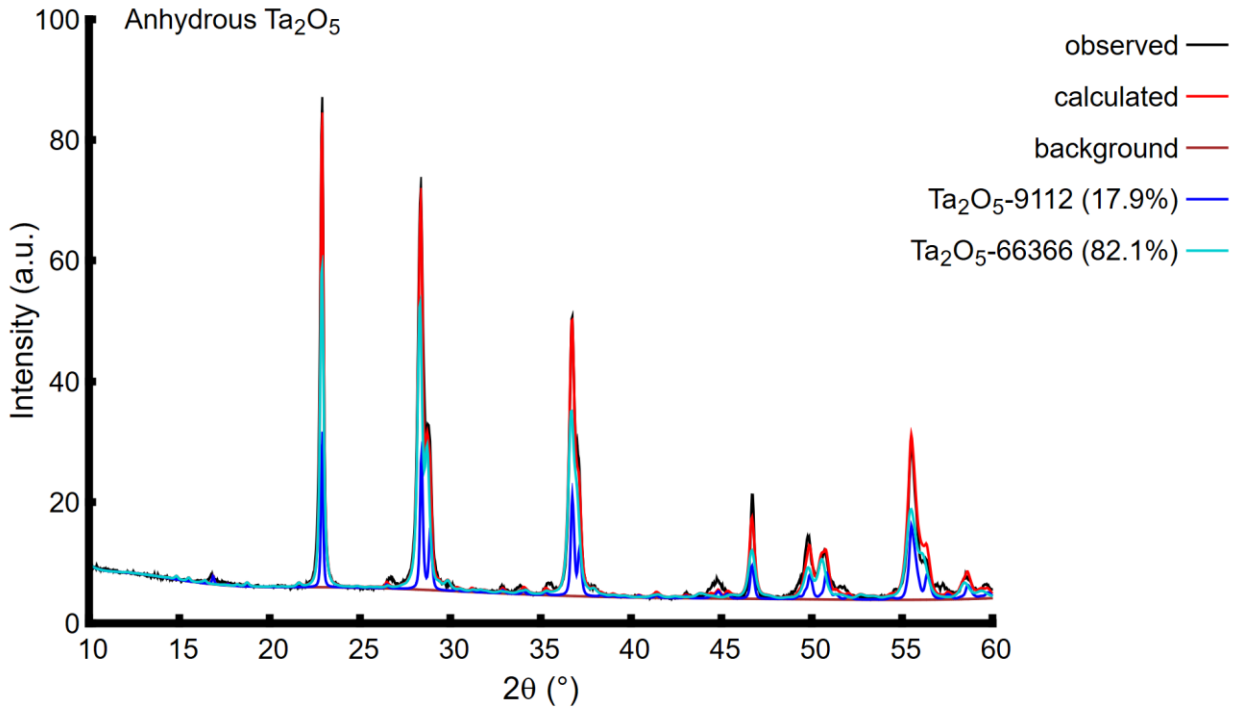

Figure S3-9. Rietveld refinement of the PXRD pattern of anhydrous Ta_2O_5. Ta_2O_5-9112 and Ta_2O_5-66366 are the orthorhombic phase of Ta_2O_5.

S3.3 Annealed polyoxometalates

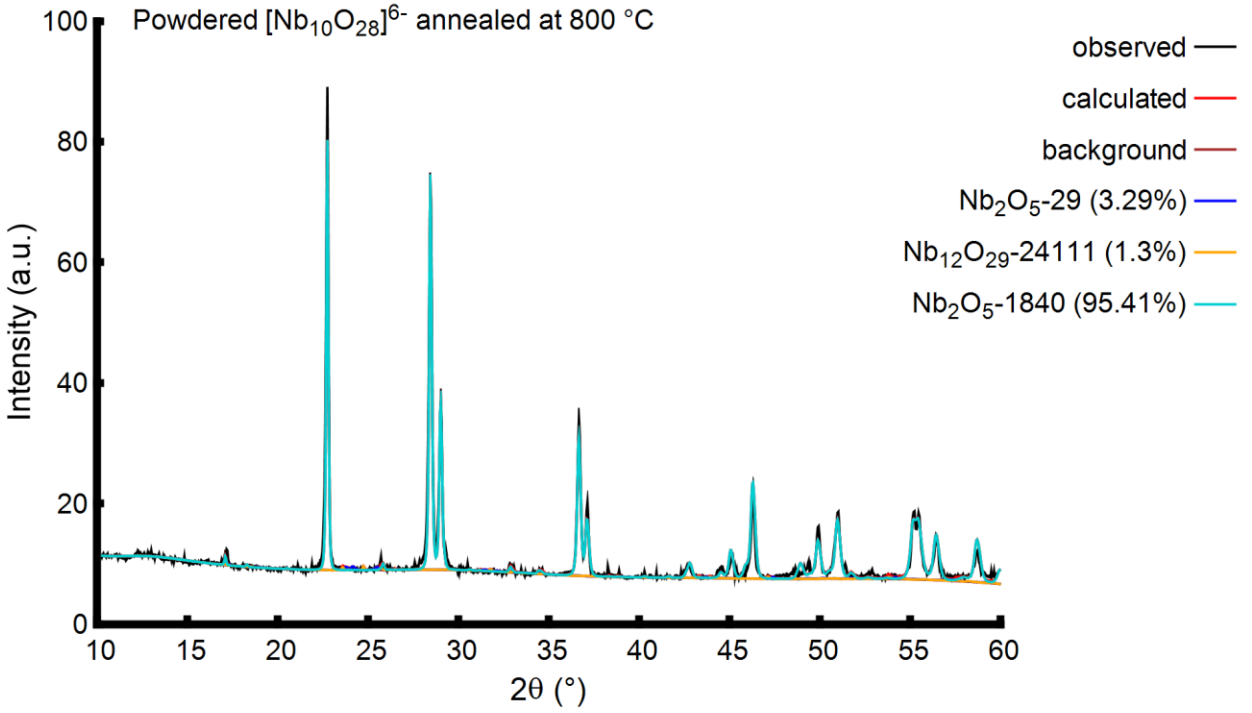

Figure S3-10. Rietveld refinement of the PXRD pattern of $[Nb_{10}O_{28}]^{6-}$ annealed at 800 °C. Nb_2O_5-29 and $Nb_{12}O_{29}$-24111 are monoclinic phases of Nb_2O_5; Nb_2O_5-1840 is the orthorhombic phase of Nb_2O_5.

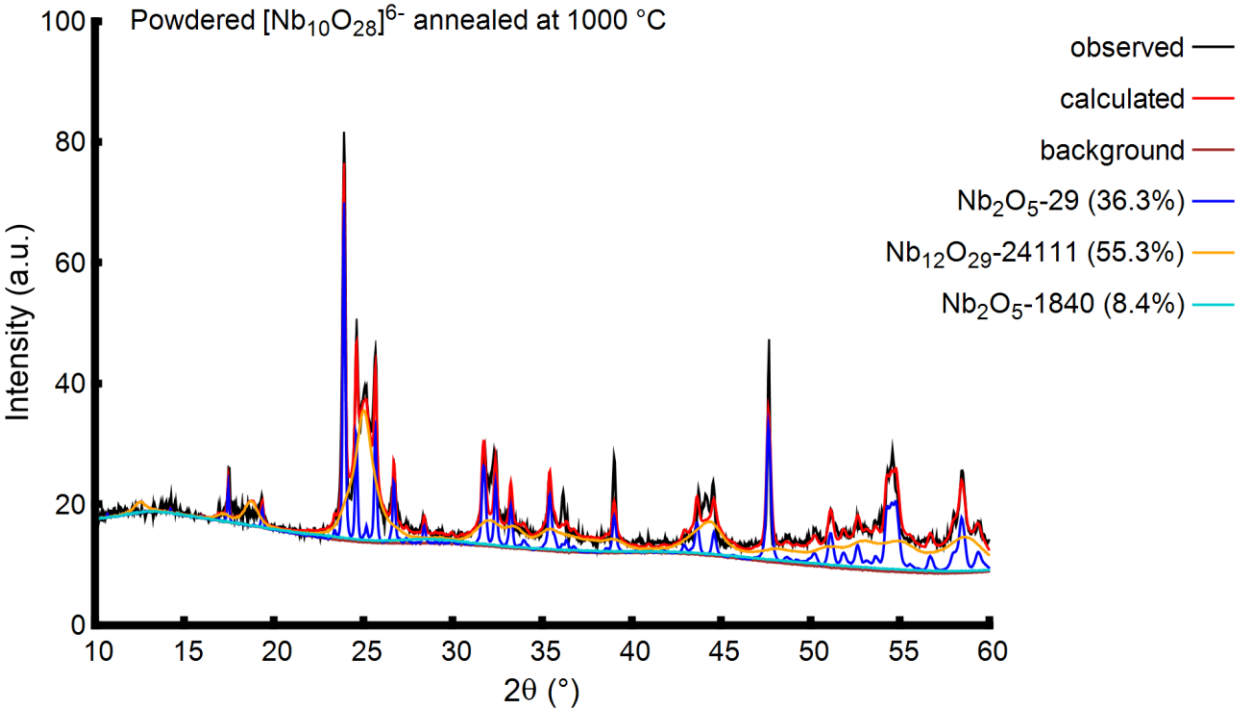

Figure S3-11. Rietveld refinement of the PXRD pattern of $[Nb_{10}O_{28}]^{6-}$ annealed at 1000 °C. Nb_2O_5-29 and $Nb_{12}O_{29}$-24111 are monoclinic phases of Nb_2O_5; Nb_2O_5-1840 is the orthorhombic phase of Nb_2O_5.

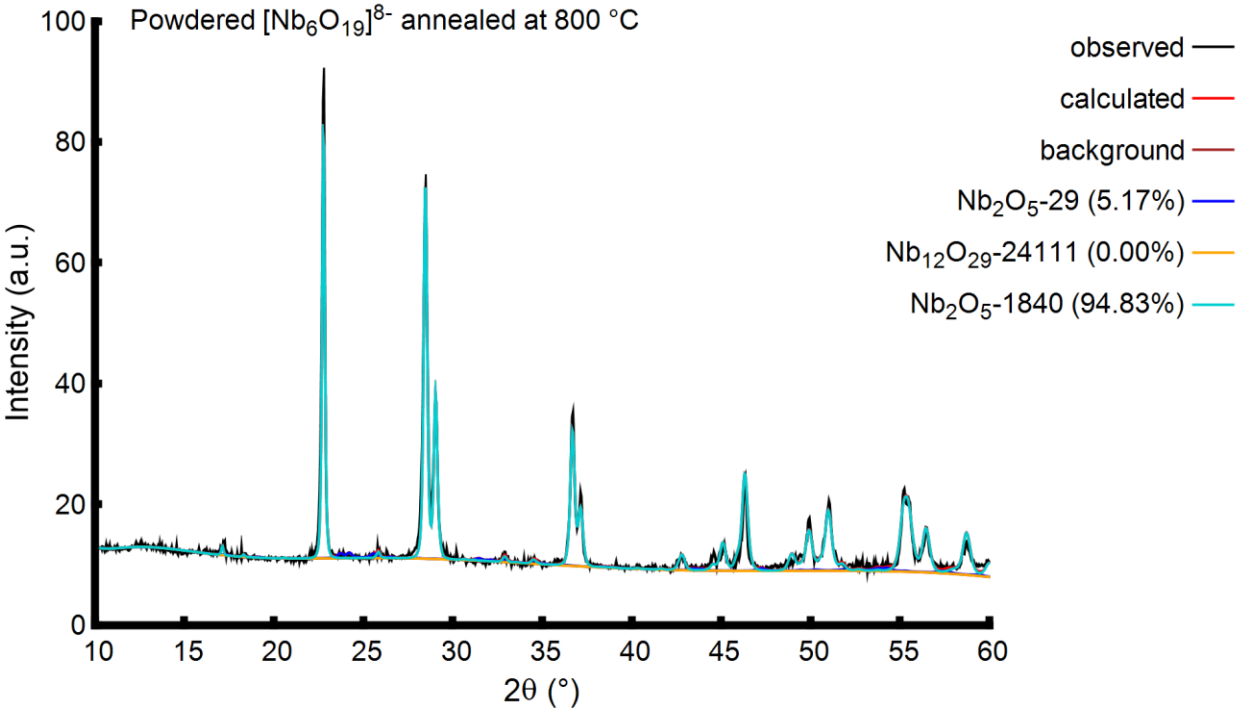

Figure S3-12. Rietveld refinement of the PXRD pattern of $[Nb_6O_{19}]^{8-}$ annealed at 800 °C. Nb_2O_5-29 and $Nb_{12}O_{29}$-24111 are monoclinic phases of Nb_2O_5; Nb_2O_5-1840 is the orthorhombic phase of Nb_2O_5.

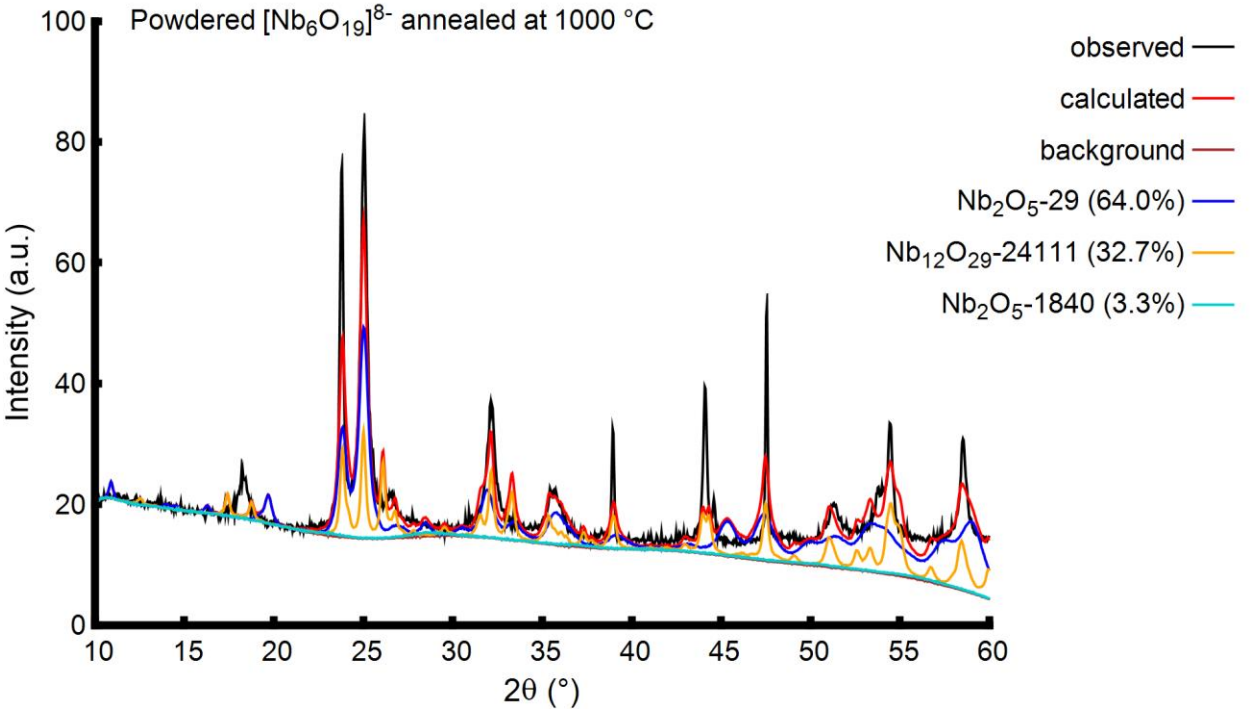

Figure S3-13. Rietveld refinement of the PXRD pattern of $[Nb_6O_{19}]^{8-}$ annealed at 1000 °C. Nb_2O_5-29 and $Nb_{12}O_{29}$-24111 are monoclinic phases of Nb_2O_5; Nb_2O_5-1840 is the orthorhombic phase of Nb_2O_5.

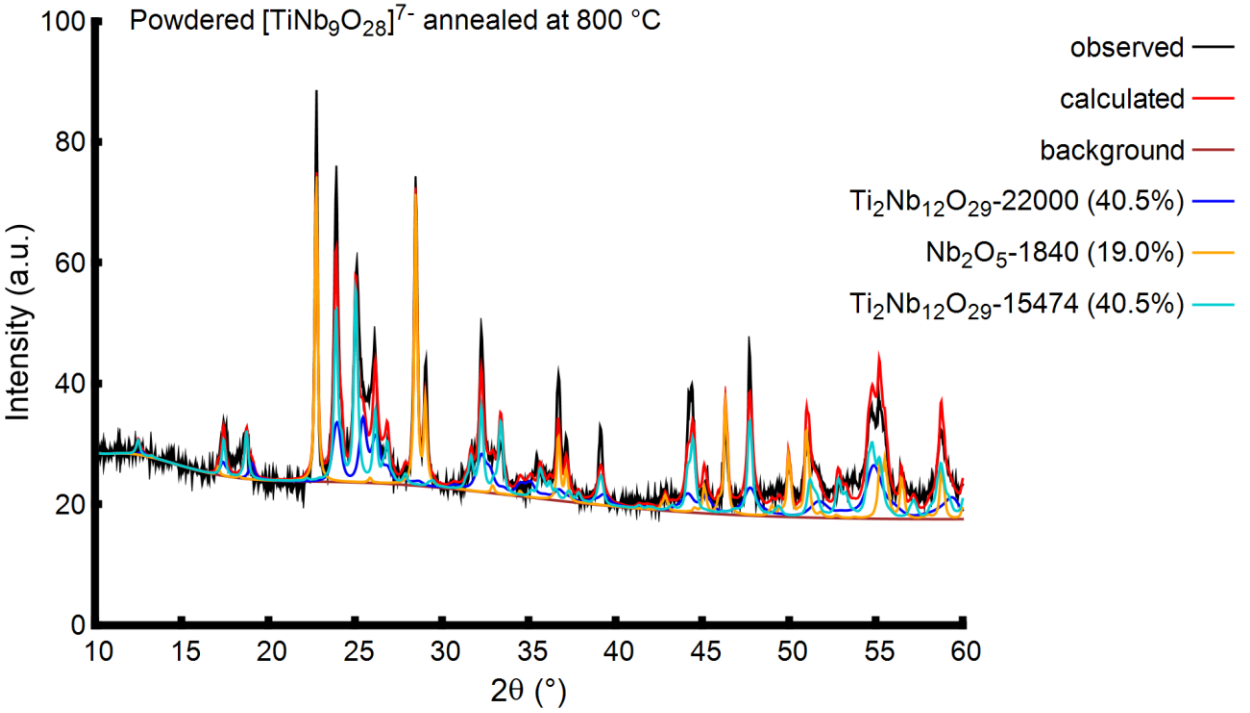

Figure S3-14. Rietveld refinement of the PXRD pattern of $[TiNb_9O_{28}]^{7-}$ annealed at 800 °C. $Ti_2Nb_{12}O_{29}$-22000 and $Ti_2Nb_{12}O_{29}$-15474 are the orthorhombic and monoclinic phases of $Ti_2Nb_{12}O_{29}$, respectively, and Nb_2O_5-1840 is the orthorhombic phase of Nb_2O_5.

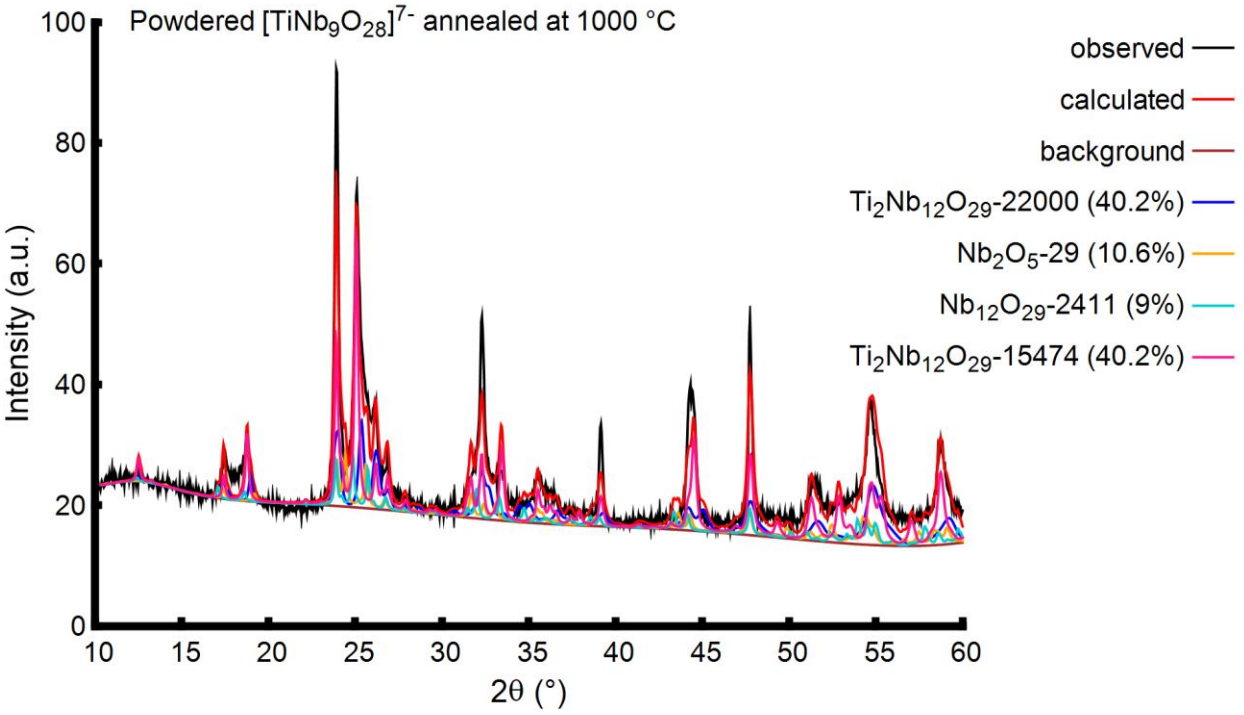

Figure S3-15. Rietveld refinement of the PXRD pattern of $[TiNb_9O_{28}]^{7-}$ annealed at 1000 °C. $Ti_2Nb_{12}O_{29}$-22000 and $Ti_2Nb_{12}O_{29}$-15474 are the orthorhombic and monoclinic phases of $Ti_2Nb_{12}O_{29}$ respectively; Nb_2O_5-29 and $Nb_{12}O_{29}$-24111 are monoclinic phases of Nb_2O_5.

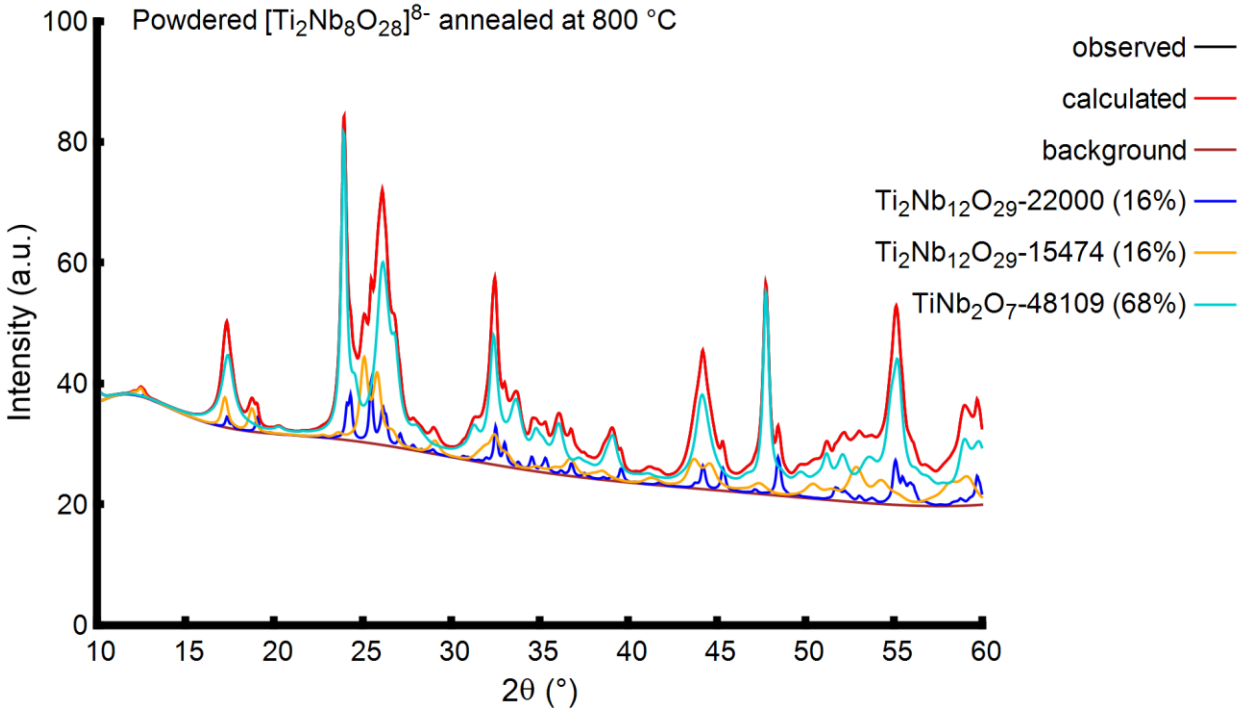

Figure S3-16. Rietveld refinement of the PXRD pattern of $[Ti_2Nb_8O_{28}]^{8-}$ annealed at 800 °C. $Ti_2Nb_{12}O_{29}$-22000 and $Ti_2Nb_{12}O_{29}$-15474 are the orthorhombic and monoclinic phases of $Ti_2Nb_{12}O_{29}$ respectively; $TiNb_2O_7$-48109 is the monoclinic phases of $TiNb_2O_7$-48109.

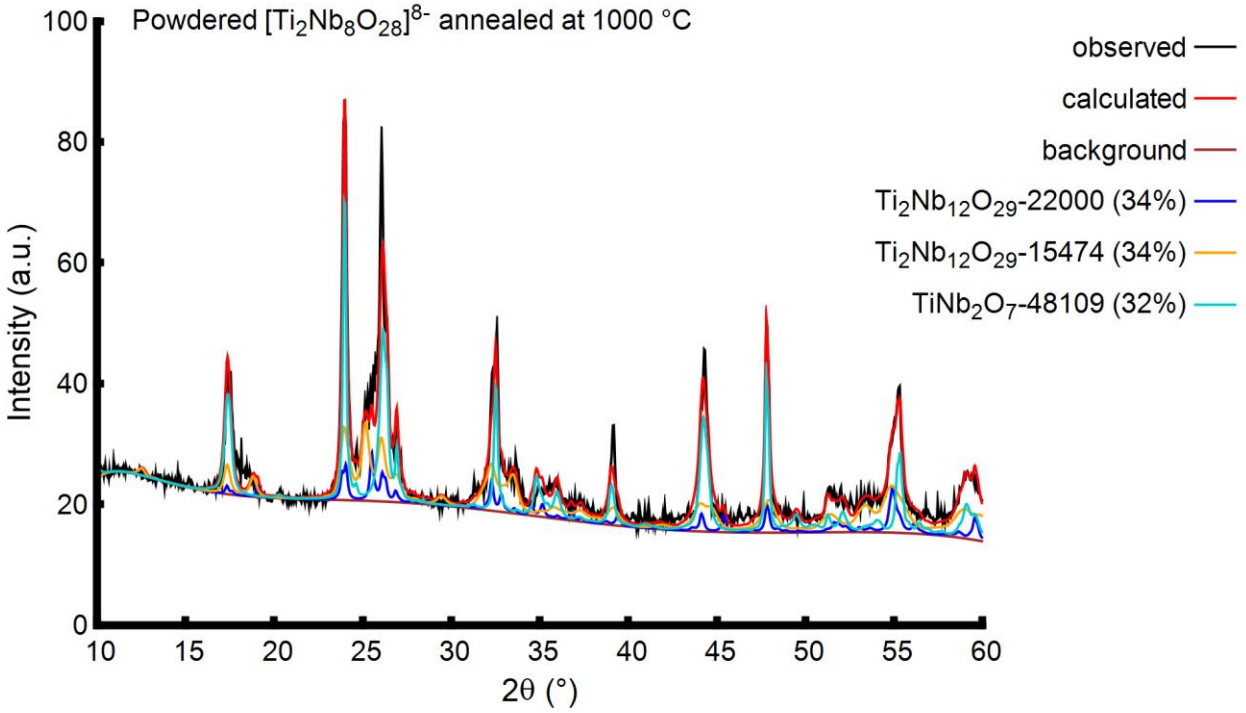

Figure S3-17. Rietveld refinement of the PXRD pattern of $[Ti_2Nb_8O_{28}]^{8-}$ annealed at 1000 °C. $Ti_2Nb_{12}O_{29}$-22000 and $Ti_2Nb_{12}O_{29}$-15474 are the orthorhombic and monoclinic phases of $Ti_2Nb_{12}O_{29}$ respectively; $TiNb_2O_7$-48109 is the monoclinic phases of $TiNb_2O_7$-48109.

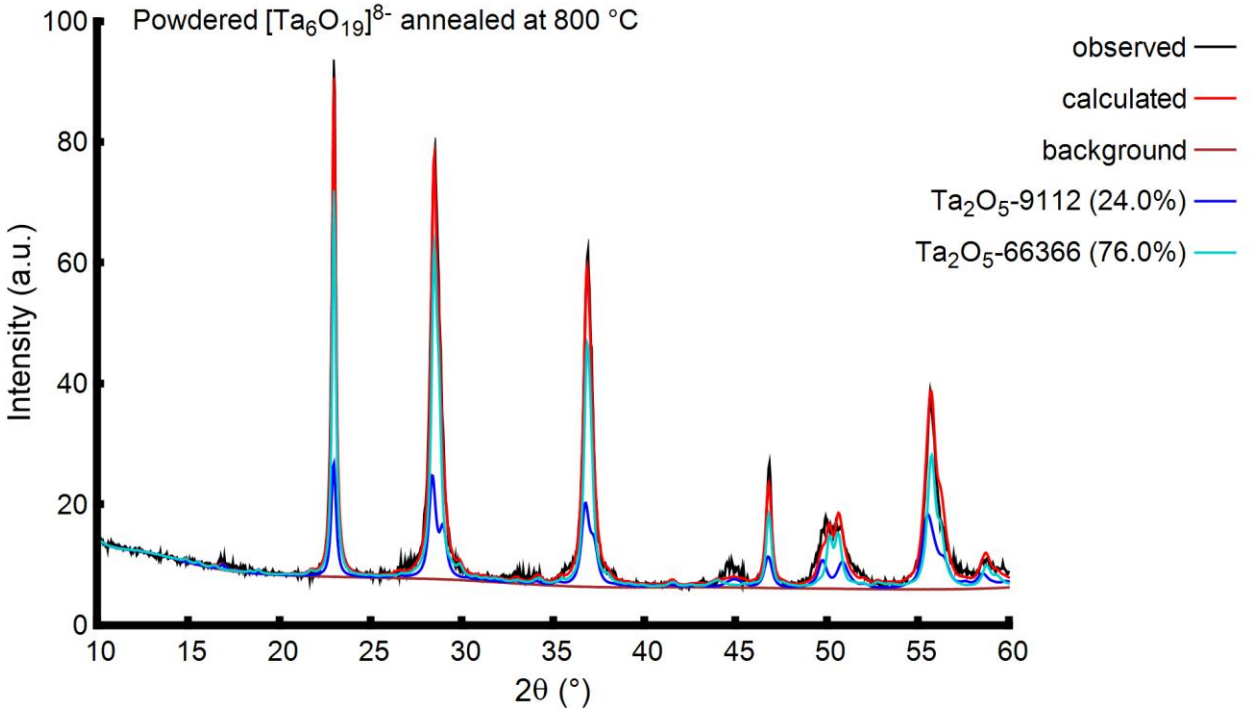

Figure S3-18. Rietveld refinement of the PXRD pattern of $[Ta_6O_{19}]^{8-}$ annealed at 800 °C. Ta_2O_5-9112 and Ta_2O_5-66366 are the orthorhombic phase of Ta_2O_5.

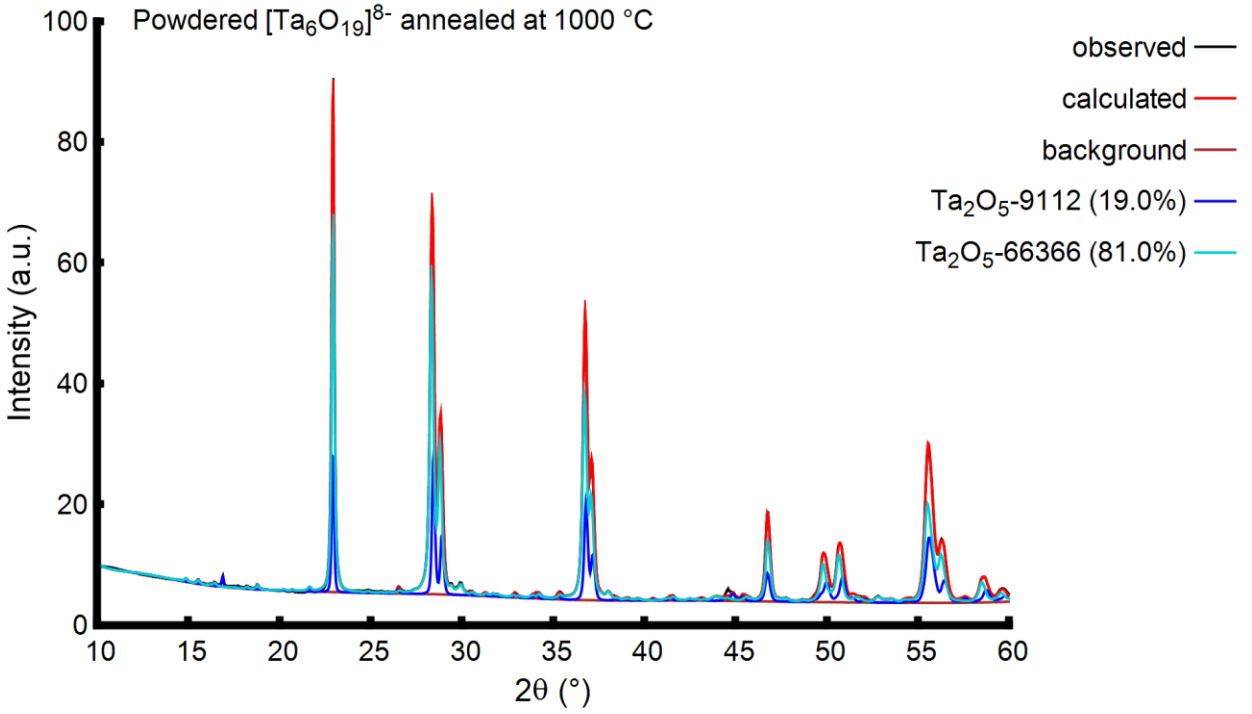

Figure S3-19. Rietveld refinement of the PXRD pattern of $[Ta_6O_{19}]^{8-}$ annealed at 1000 °C. Ta_2O_5-9112 and Ta_2O_5-66366 are the orthorhombic phase of Ta_2O_5.

S4. SEM

Table S4-1. Thickness (by SEM) and roughness (by AFM) of polyoxometalate films annealed at 800 °C and 1,000 °C.

Polyoxometalate (0.2 M)	**Temperature (°C)**	**Oxide formed**	**Thickness (nm)**	**Root mean square roughness (nm)**
$[Nb_{10}O_{28}]^{6-}$	800	ortho-Nb_2O_5	235±5	±24.0
	1000	mono-Nb_2O_5	199±6[a] 442±44 [b]	±54.9
$[TiNb_9O_{28}]^{7-}$	800	$Ti_2Nb_{12}O_{29}$	363±5	±17.7
	1000	$Ti_2Nb_{12}O_{29}$	172±3 [a] 262±18[b]	±35.3
$[Ti_2Nb_8O_{28}]^{8-}$	800	$TiNb_2O_7$	576±9	±21.6
	1000	$TiNb_2O_7$	169±1 [a] 383±23 [b]	±13.8
$[Nb_6O_{19}]^{8-}$	800	ortho-Nb_2O_5	287±7	±9.02
	1000	mono-Nb_2O_5	188±8 [a] 228 ±24[b]	±35.6
$[Ta_6O_{19}]^{8-}$	800	ortho-Ta_2O_5	266±2	±9.61
	1000	ortho-Ta_2O_5	167±5 [a] 250±4 [b]	±5.8

[a] lower layer and [b] upper layer

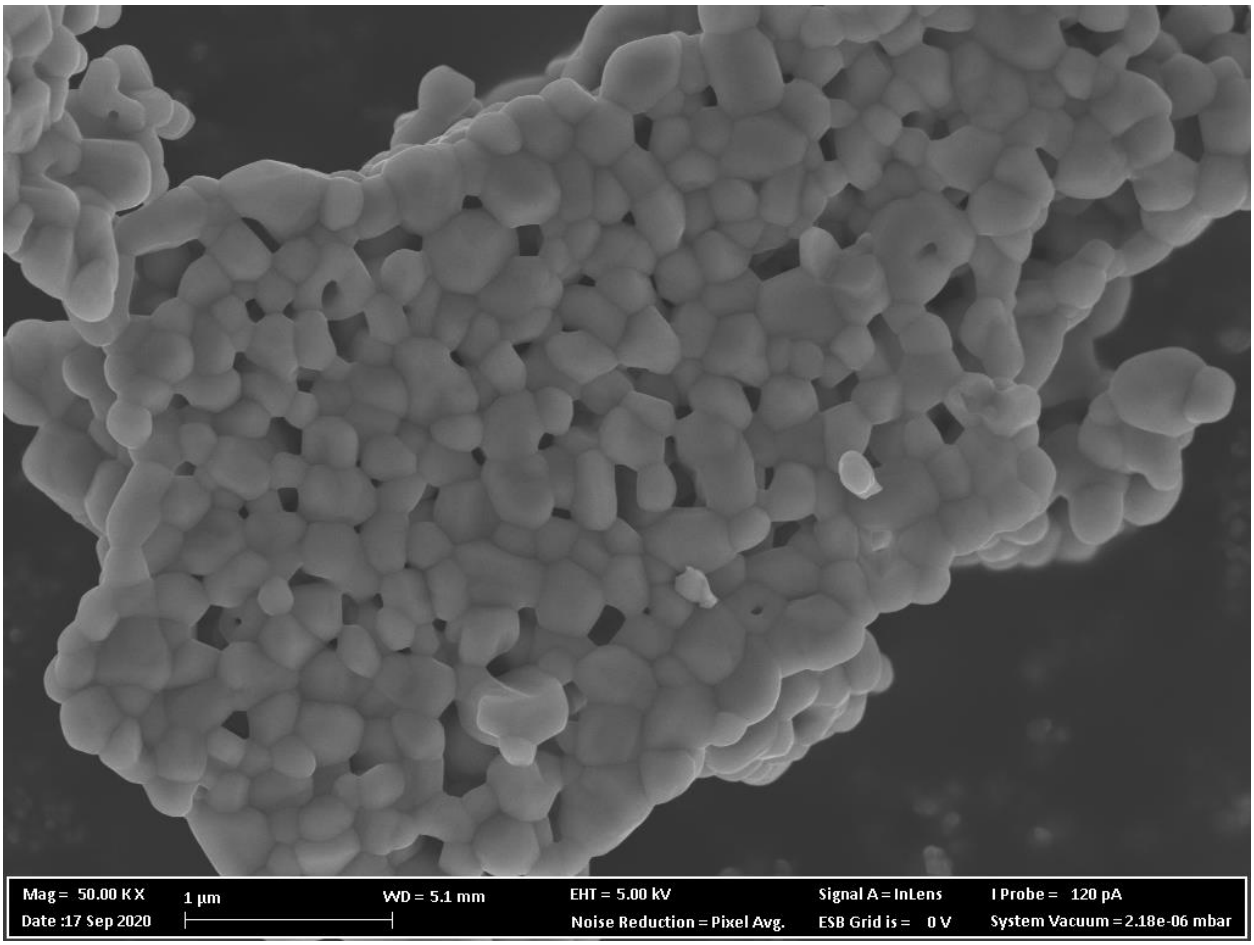

Figure S4-1. SEM image of powdered $[Nb_{10}O_{28}]^{6-}$ annealed at 800 °C.

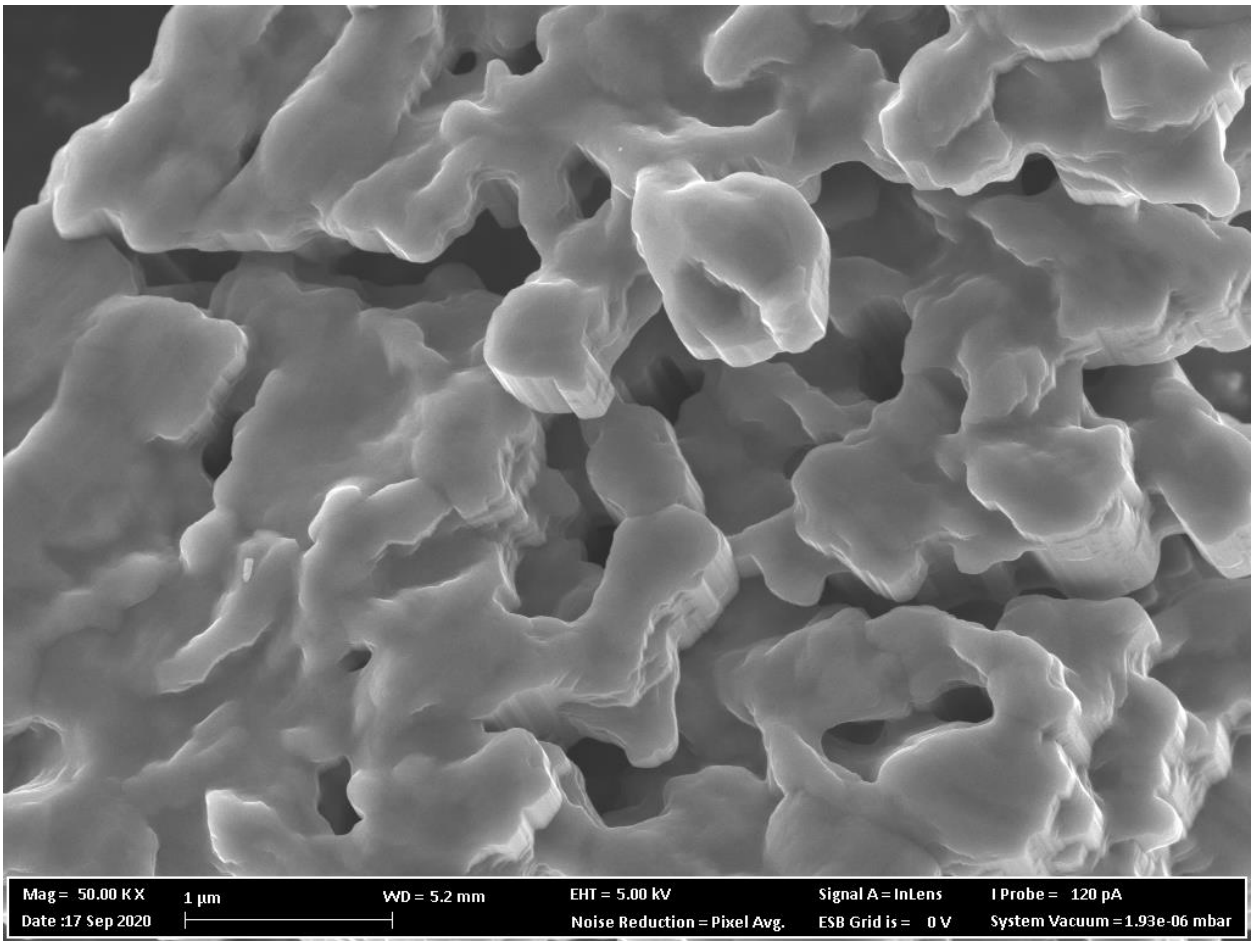

Figure S4-2. SEM image of powdered $[Nb_{10}O_{28}]^{6-}$ annealed at 1000 °C.

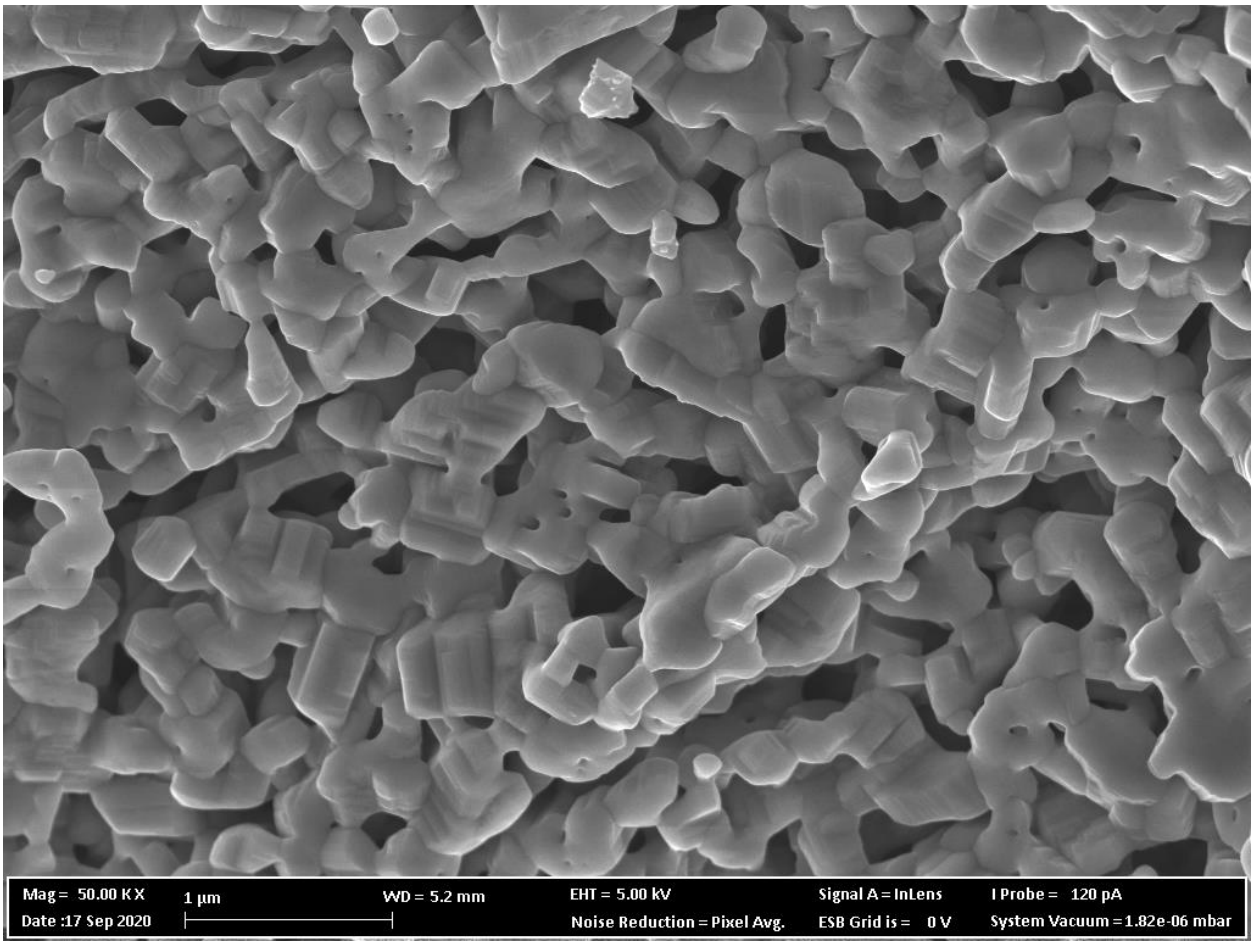

Figure S4-3. SEM image of powdered $[TiNb_9O_{28}]^{7-}$ annealed at 1000 °C.

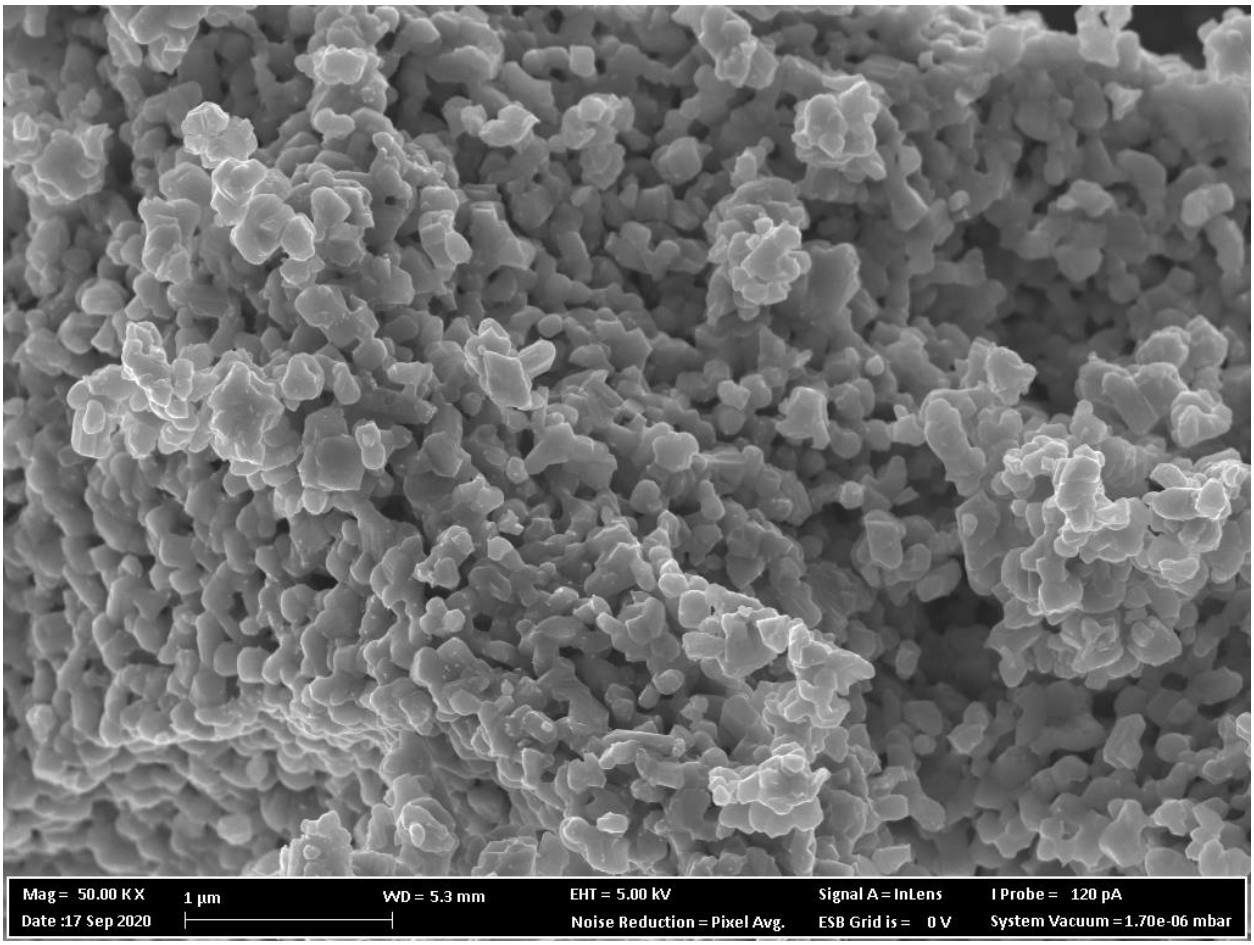

Figure S4-4. SEM image of powdered $[Ti_2Nb_8O_{28}]^{8-}$ annealed at 1000 °C

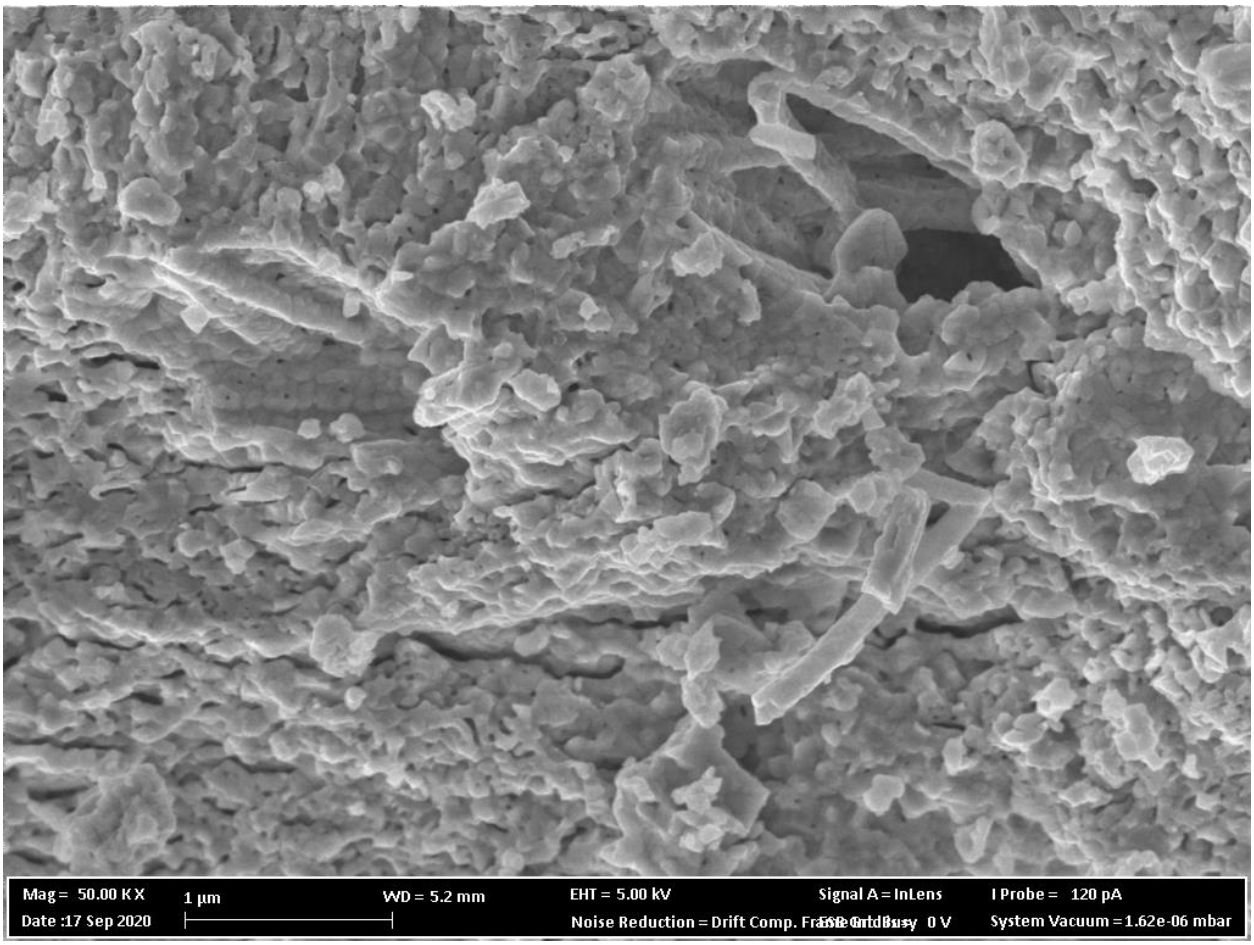

Figure S4-5. SEM image of powdered $[Ta_6O_{19}]^{8-}$ annealed at 1000 °C

S5. EDS

Table S5-1. Atomic composition of annealed polyoxometalate films

Polyoxometalate[a]	Calculated composition %	Atomic composition (%) of films relative to temperature (°C)			
		200	400	800	1000
$[N(CH_3)_4]_6[Nb_{10}O_{28}]\cdot 2H_2O$	4.09 (H) 15.51 (C) 4.52 (N) 25.85 (O) 50.03 (Nb)	30.12 (C) 5.36 (N) 33.27 (O) 18.96 (Si) 12.29 (Nb)	8.31 (C) 63.66 (O) 5.2 (Si) 22.81 (Nb)	1.21 (C) 58.69 (O) 16.16 (Si) 23.93 (Nb)	0.2 (C) 63.89 (O) 10.8 (Si) 25.11 (Nb)
$[N(CH_3)_4]_7[TiNb_9O_{28}]\cdot 3H_2O$	4.73 (H) 17.65 (C) 5.15 (N) 26.05 (O) 2.51 (Ti) 43.91 (Nb)	28.16 (C) 47.37 (O) 6.55 (Si) 1.71 (Ti) 16.21 (Nb)	7.06 (C) 60.15 (O) 10.10 (Si) 2.44 (Ti) 20.24 (Nb)	0.50 (C) 60.85 (O) 14.13 (Si) 2.24 (Ti) 22.28 (Nb)	0.88 (C) 63.71 (O) 10.03 (Si) 2.43 (Ti) 22.95 (Nb)
$[N(CH_3)_4]_8[Ti_2Nb_8O_{28}]\cdot 6H_2O$	5.44 (H) 19.33 (C) 5.64 (N) 27.38 (O) 4.82 (Ti) 37.4 (Nb)	22.32 (C) 52.05 (O) 3.41 (Si) 6.49 (Ti) 15.74 (Nb)	6.17 (C) 63.4 (O) 4.08 (Si) 7.67 (Ti) 18.68 (Nb)	2.71 (C) 64.73 (O) 3.75 (Si) 8.29 (Ti) 20.52 (Nb)	65.84 (O) 5.39 (Si) 8.40 (Ti) 20.37 (Nb)
$[N(CH_3)_4]_8[Nb_6O_{19}]\cdot 2H_2O$[b]	6.71 (H) 25.78 (C) 7.52 (N) 22.56 (O) 37.42 (Nb)	25.43 (C) 32.8 (O) 30.13 (Si) 11.64 (Nb)	3.13 (C) 49.99 (O) 29.41 (Si) 17.46 (Nb)	1.66 (C) 47.85 (O) 32.24 (Si) 18.25 (Nb)	56.71 (O) 24.64 (Si) 18.64 (Nb)
$[N(CH_3)_4]_8[Ta_6O_{19}]$[b]	4.85 (H) 19.38 (C) 5.65 (N) 15.34 (O) 54.78 (Ta)	17.2 (C) 55.13 (O) 7.45 (Si) 20.22 (Ta)	8.11 (C) 55.49 (O) 14.60 (Si) 21.80 (Ta)	61.74 (O) 14.15 (Si) 24.11 (Ta)	59.77 (O) 16.42 (Si) 23.81 (Ta)

[a] 0.2 M, [b] Synthesised according to previous microwave synthesis of hexaniobate and hexatantalate.[1]

S6. AFM

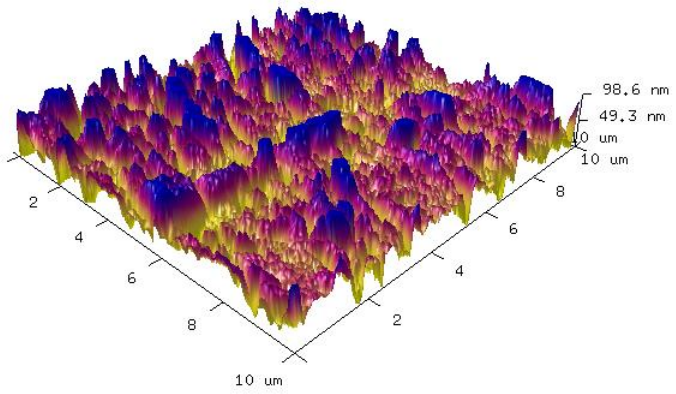

Figure S6-1. AFM image of four successively deposited layers of $[Nb_{10}O_{28}]^{6-}$ film annealed at 800 °C.

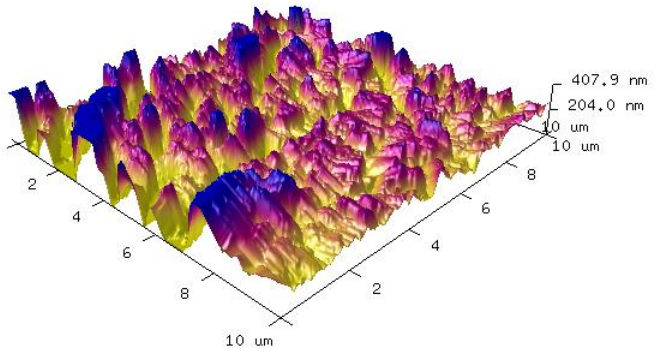

Figure S6-2. AFM image of four successively deposited layers of $[Nb_{10}O_{28}]^{6-}$ film annealed at 1000 °C.

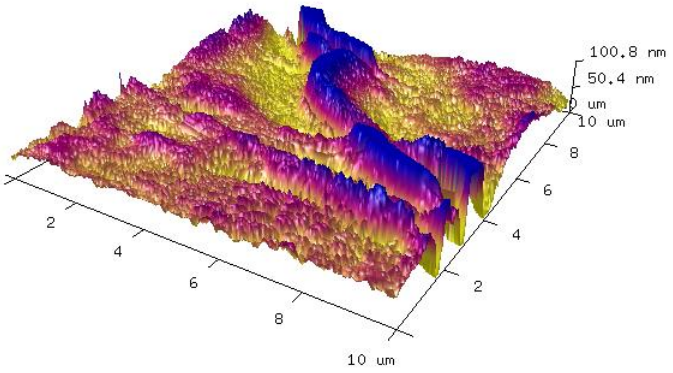

Figure S6-3. AFM image of four successively deposited layers of $[Nb_6O_{19}]^{8-}$ film annealed at 800 °C.

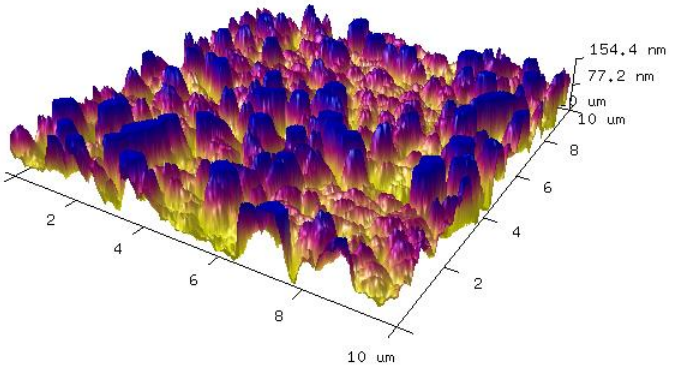

Figure S6-4. AFM image of four successively deposited layers of $[Nb_6O_{19}]^{8-}$ film annealed at 1000 °C.

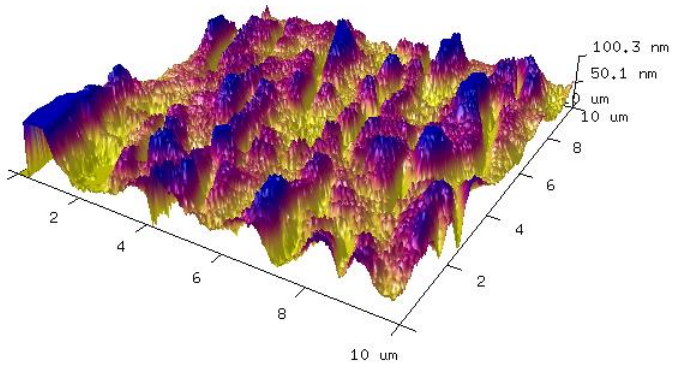

Figure S6-5. AFM image of four successively deposited layers of $[TiNb_9O_{28}]^{7-}$ film annealed at 800 °C.

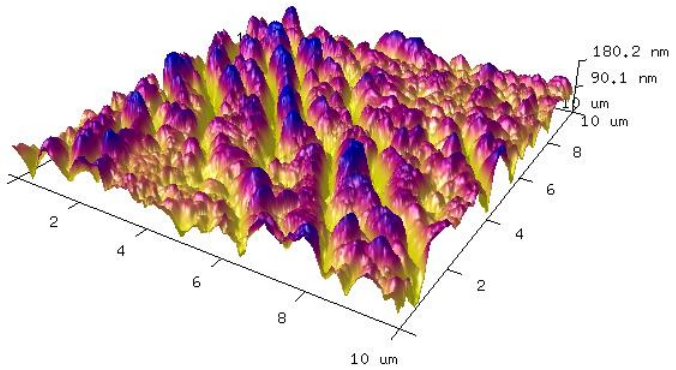

Figure S6-6. AFM image of four successively deposited layers of $[TiNb_9O_{28}]^{7-}$ film annealed at 1000 °C.

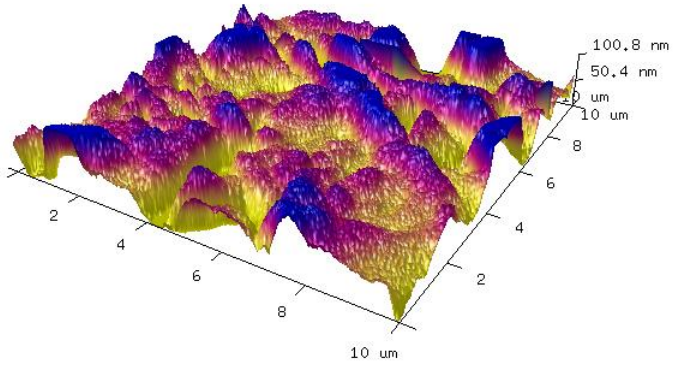

Figure S6-7. AFM image of four successively deposited layers of $[Ti_2Nb_8O_{28}]^{8-}$ film annealed at 800 °C.

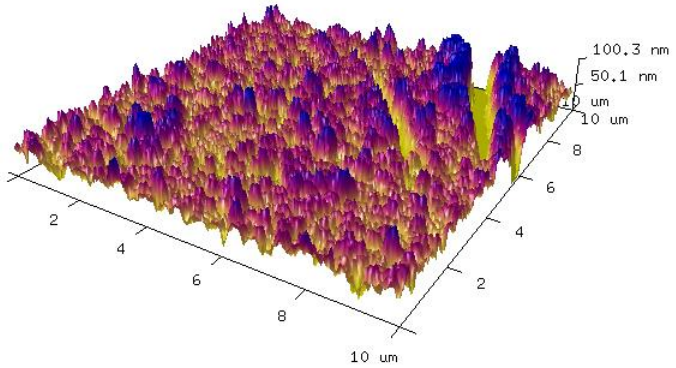

Figure S6-8. AFM image of four successively deposited layers of $[Ti_2Nb_8O_{28}]^{8-}$ film annealed at 1000 °C.

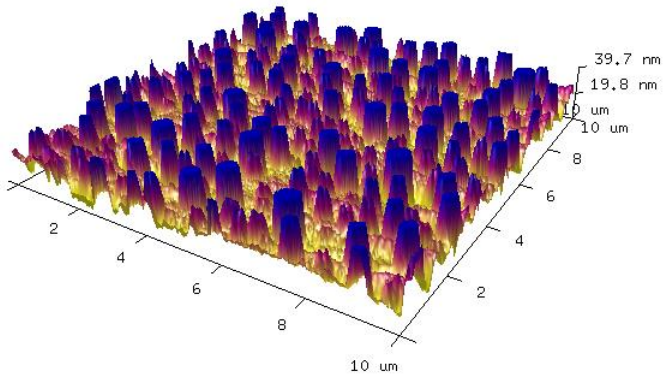

Figure S6-9. AFM image of four successively deposited layers of $[Ta_6O_{19}]^{8-}$ film annealed at 800 °C.

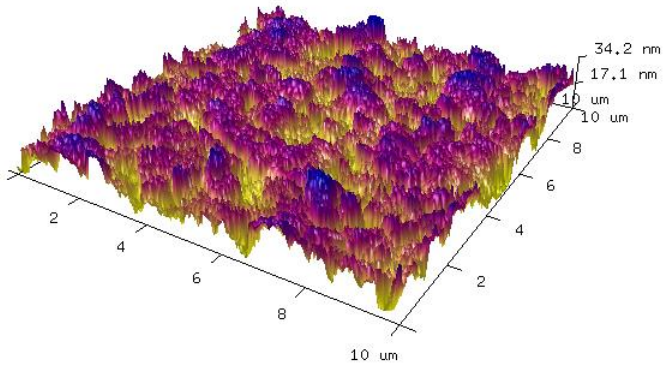

Figure S6-10. AFM image of four successively deposited layers of $[Ta_6O_{19}]^{8-}$ film annealed at 1000 °C.

S7. ^{17}O-NMR spectroscopy of POMs

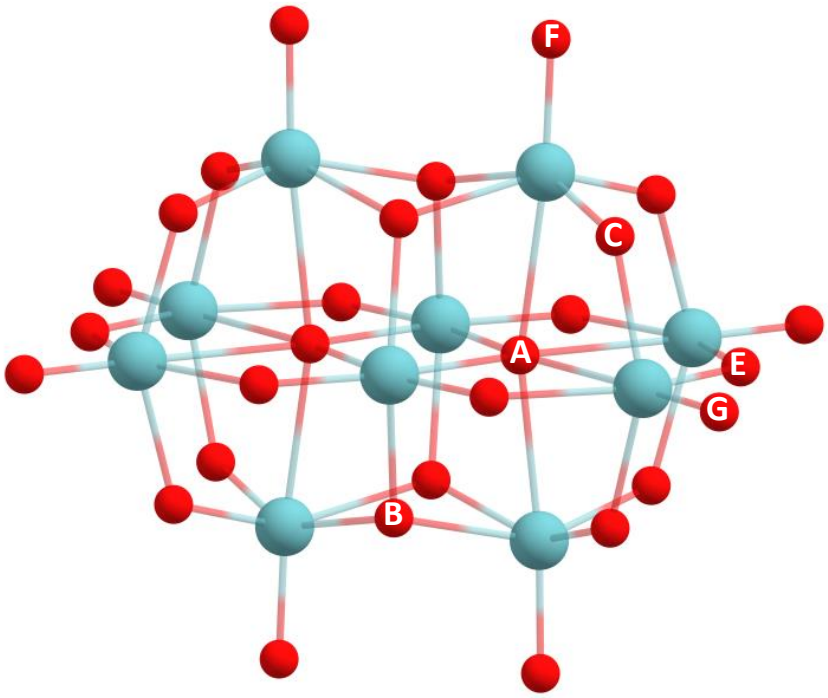

Figure S7-1. The $[Nb_{10}O_{28}]^{6-}$ ion with each symmetry unique oxygen labelled A: μ_6-O; B: μ_3-O; C-E: μ_2-O; F-G: η=O. Red and light blue spheres represent niobium and oxygen atoms respectively.

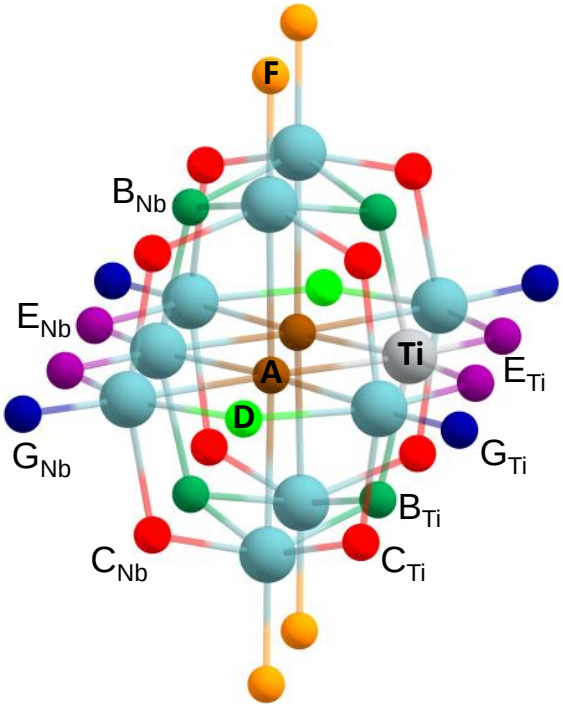

Figure S7-2. Side view of the $[TiNb_9O_{28}]^{7-}$ ion with each symmetry unique oxygen labelled A: μ_6-O; B_{Nb} and B_{Ti}: μ_3-O; C_{Nb} and C_{Ti}: μ_2-O; D: μ_2-O; E_{Nb} and E_{Ti}: μ_2-O; F: η=O; G_{Nb} and G_{Ti}: η=O. Red, grey and light blue spheres represent oxygen, titanium and niobium atoms respectively.

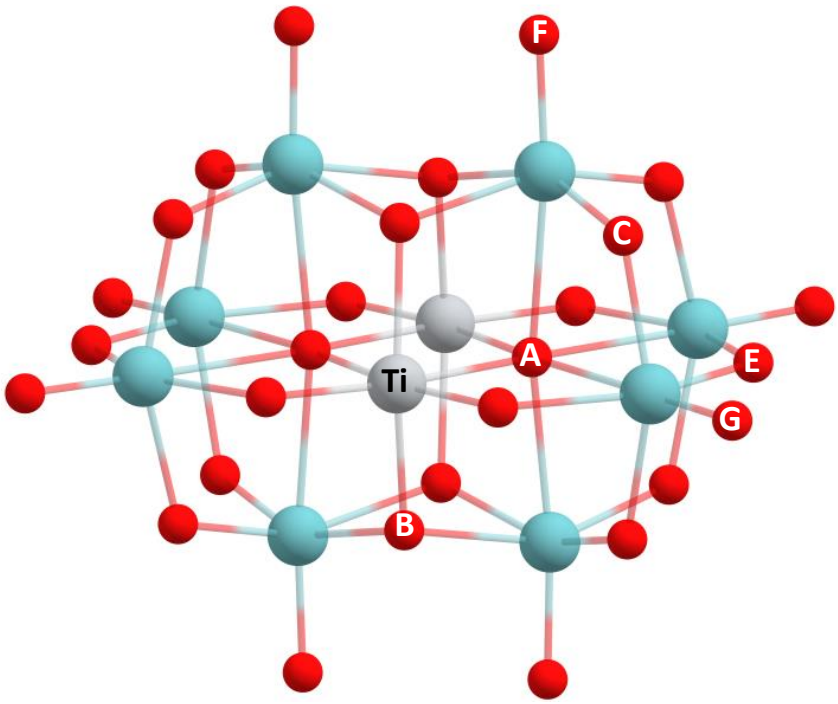

Figure S7-3. The $[Ti_2Nb_{10}O_{28}]^{8-}$ ion with each symmetry unique oxygen labelled A: μ_6-O; B: μ_3-O; C-E: μ_2-O; F-G: η=O. Red, grey and light blue spheres represent oxygen, titanium and niobium atoms respectively.

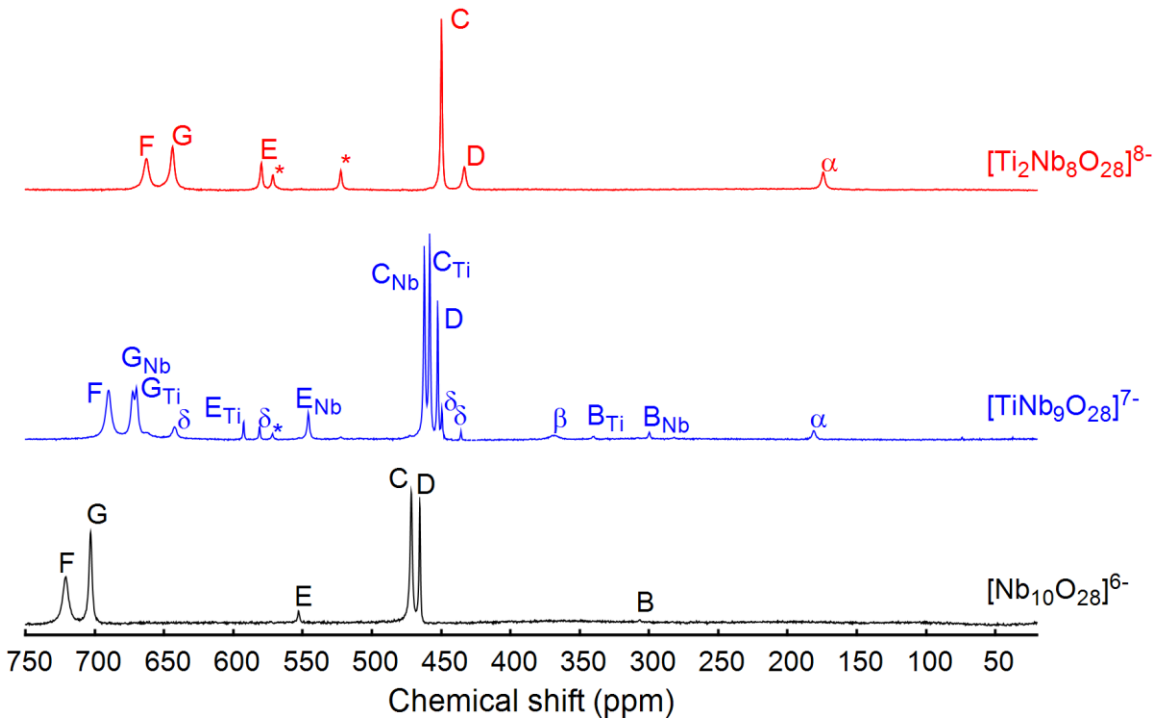

Figure S7-4. ^{17}O-NMR spectra of $[Nb_{10}O_{28}]^{6-}$ (black line), $[TiNb_9O_{28}]^{7-}$ (blue line) and $[Ti_2Nb_8O_{28}]^{8-}$ (red line) in unbuffered 20% ^{17}O enriched H_2O. $^{\alpha}$Carbonate is present at 180.5 ppm;[3] $^{\beta}$the broad peak at 368.3 ppm is attributable to protonation of the μ_2-O at site b of $[Nb_6O_{19}]^{8-}$and is a known impurity in the synthesis of $TiNb_9$;[1, 4, 5] $^{\delta}$peaks are attributable to $[Ti_2Nb_8O_{28}]^{8-}$;[4] *impurities in the NMR solvent which has been recycled.

Table S7-1. Oxygen chemical shifts (ppm) for $[Nb_{10}O_{28}]^{6-}$, $[TiNb_9O_{28}]^{7-}$ and $[Ti_2Nb_8O_{28}]^{8-}$ in unbuffered solutions of recycled 20% ^{17}O enriched H_2O.

	[a]Chemical shift (ppm)		
Site of chemical shift	**$[Nb_{10}O_{28}]^{6-}$**	**$[TiNb_9O_{28}]^{7-}$**	**$[Ti_2Nb_8O_{28}]^{8-}$**
μ_3-O at B	306.6	299.8 (B_{Nb})	Not observed
		340.2 (B_{Ti})	
μ_2-O at D	465.3	452.5	433.3
μ_2-O at C	471.5	458.3 (C_{Ti})	449.8
		462.2 (C_{Nb})	
μ_2-O at E	552.9	545.9 (E_{Nb})	579.8
		592.6 (E_{Ti})	
η=O at G	703	670.2 (G_{Ti})	644.1
		672.5 (G_{Nb})	
η=O at F	720.9	690.1	662.8

[a]Based on previous assignments by Villa *et al.*[4]

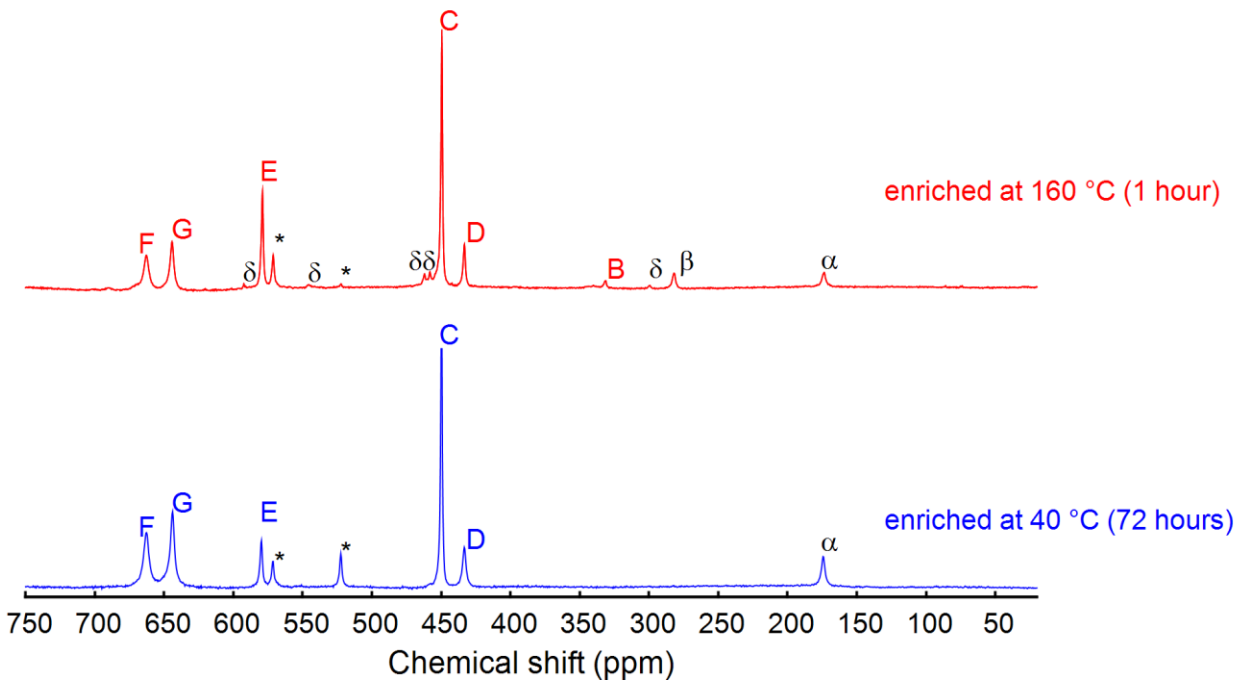

Figure S7-5. ^{17}O-NMR spectra of $[Ti_2Nb_8O_{28}]^{8-}$ enriched at 40 °C for 72 hours (bottom) and 160 °C for 1 hour (top) in unbuffered recycled 20% ^{17}O-enriched H_2O. [α]Carbonate is present at 180.5 ppm;[3] [β]the $[Ti_{12}Nb_6O_{44}]^{10-}$ ion;[4] [δ]peaks are attributable to $[TiNb_9O_{28}]^{7-}$;[4] * impurities present in the recycled NMR solvent.

S8. UV-visible spectroscopy

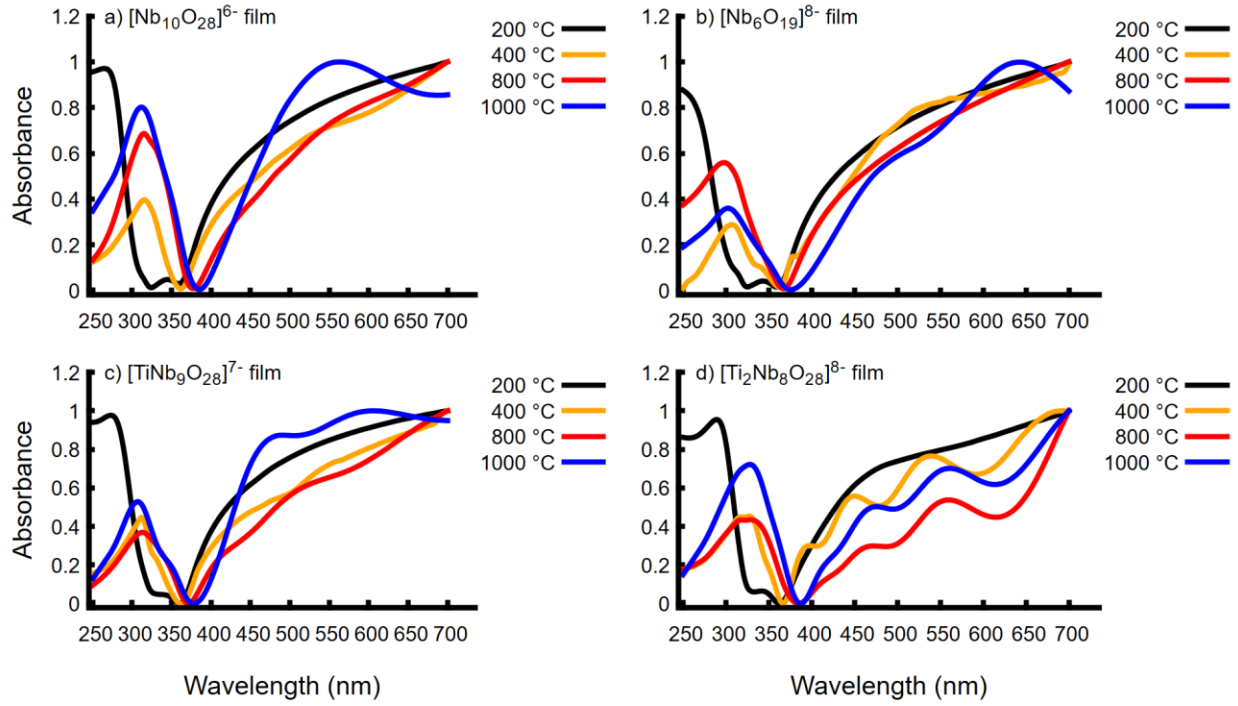

Figure S8-1. UV-visible spectra of Nb_{10} (a), Nb_6 (b), $TiNb_9$ (c) and Ti_2Nb_8 (d) films annealed at 200 – 1000 °C. Films annealed at temperatures ≥800 °C exhibit greater absorption within the UV region compared to lower temperatures.

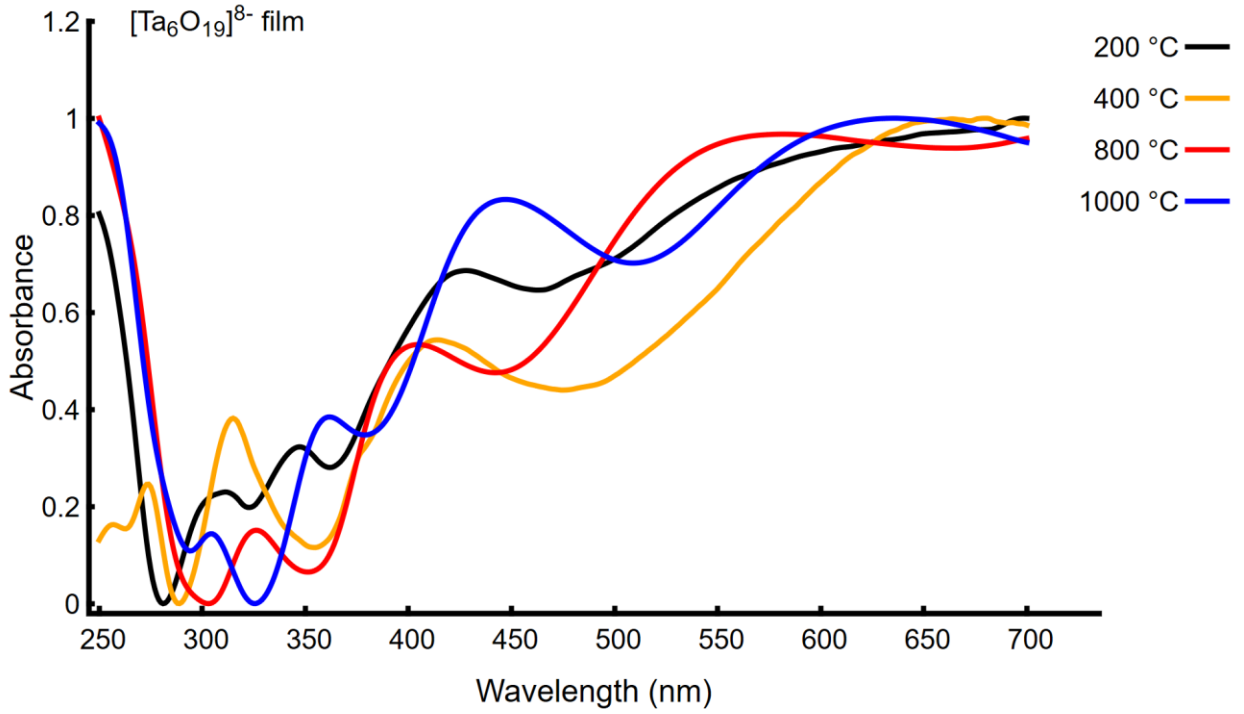

Figure S8-2. UV-visible spectra of Ta_6 films annealed at 200 – 1000 °C.

References

1. M. A. Rambaran, M. Pascual-Borràs and C. A. Ohlin, *Eur. J. Inorg. Chem.*, 2019, DOI: 10.1002/ejic.201900750, 3913-3918.
2. N. Doebelin and R. Kleeberg, *J. Appl. Cryst.*, 2015, **48**, 1573-1580.
3. D. L. Clark, T. W. Newton, P. D. Palmer and B. D. Zwick, *^{13}C and ^{17}O NMR binding constant studies of uranyl carbonate complexes in near-neutral aqueous solution Yucca Mountain Project Milestone Report 3351*, United States, 1995.
4. E. M. Villa, C. A. Ohlin and W. H. Casey, *J. Am. Chem. Soc.*, 2010, **132**, 5264-5272.
5. R. Sharma, J. Zhang and C. A. Ohlin, *Phys. Chem. Chem. Phys.*, 2016, **18**, 8235-8241.